



Metallization in hydrogenlike systems under high pressureNeetik Mukherjee ^{1,*}, Chandra N. Patra,^{2,†} and Amlan K. Roy ^{1,‡}¹*Department of Chemical Sciences, IISER Kolkata, Mohanpur-741246, Nadia, West Bengal, India*²*Theoretical Chemistry Section, Chemistry Group, Bhabha Atomic Research Centre, Mumbai-400085, India*

(Received 18 July 2022; accepted 9 September 2022; published 27 September 2022)

Almost a century ago, it was proposed that solid hydrogen could become metallic at sufficiently high pressure. Five years back, scientists observed an insulator to metal transition in liquid deuterium experimentally, at around 300 GPa. The present work discusses and demonstrates the metal-like behavior in elemental hydrogen under various plasma environments. At the onset, the Herzfeld criterion is invoked to examine such characteristics in such plasmas under multimegabar pressure. However, a thorough study using this condition can only explain the metal-like pattern in *s*-wave states under a shell-confined condition (the system is trapped inside two concentric spheres with inner and outer radii R_a, R_b). Moreover, using this criterion, it is not possible to explain such phenomena in (i) confined systems (involving all ℓ) and (ii) for $\ell \neq 0$ states in a shell-confined environment. Here this criterion is modified to incorporate the environmental conditions (nuclear charge, screening constant, boundary conditions) by utilizing several independent and generalized scaling concepts. The present condition can interpret a metallic pattern in confined and shell-confined plasmas connecting $\ell \geq 0$ states. Further, a different descriptor is proposed therefrom. The role of pressure in defining such a descriptor is also examined. Pilot calculations are performed using Debye Hückel, exponential screen Coulomb potential, and ion-sphere plasmas. The relevance of the shell-confined model in the context of plasmas is elaborated. Additionally, an attempt is made to investigate the metallic character in H-like systems embedded in fullerene under high pressure.

DOI: [10.1103/PhysRevA.106.032812](https://doi.org/10.1103/PhysRevA.106.032812)**I. INTRODUCTION**

Hydrogen is the most abundant material in the universe. Being the lightest element, its behavioral pattern is strongly affected by the nuclear quantum mechanical effect. As a consequence, several unique characteristics are observed in it. It has massive quantum *zero point energy*. It forms one of the strongest bonds (H–H) in chemistry. Further, as the simplest element, it acts as a classical testing ground for physics, chemistry, geosciences, and material science. At an ambient condition, it can readily form compounds with almost every element in the periodic table. It forms water with oxygen—the main requirement of life to survive. At 180 GPa and 260 °K, it combines with lanthanum to form the highest claimed temperature superconductor LaH₁₀ [1,2]. It has been found that the Jovian planets, such as Jupiter, Saturn, etc., mainly consist of highly condensed metallic hydrogen in a plasma state [3,4], which is responsible for their extraordinary magnetic field [5]. In the near future, hydrogen fuel cells may become the main source of energy for industrial and transportation purposes.

Materials under significantly high pressure undergo fascinating changes in their structure, bonding, and properties that have important implications for the fundamental science, material, and technology [6,7]. In the first half of the 20th

Century, the famous Irish physicist Bernal proposed that “all substances go over under very high pressures into metallic or valence lattice” [8]. Synthesis of metallic hydrogen under extreme conditions will provide us with the lightest metal on the earth. Most importantly, it was proposed that at very high pressure, hydrogen might undergo a transition from an insulator to a monatomic metal. Particularly at that characteristic pressure, it possesses a unique density with a negative energy, but much higher than that of its ordinary form [8,9].

In 1968, it was proposed that metallic modification of hydrogen may guide us to a high-temperature superconductor [10]. With an increase in external pressure, conductivity increases and resistivity decreases [11]. An explicit theoretical investigation elicits that at around 400 GPa and 0 °K, hydrogen is entirely in a new state of matter. Moreover, depending upon the applied magnetic field, such a state can be superfluid and superconducting [12,13]. Thirty years ago, the first claim about the metallization of hydrogen at around 200 GPa was made in [14,15]. In this context, the authors used certain Raman spectroscopic observations to explain this phenomenon. Later, with the improvement of experimental techniques, it was found that such outcomes appeared due to the instrumental noise. About 10 years ago, a new demand surfaced that scientists have observed “liquid atomic metallic hydrogen” at above 260 GPa [16]. They delineated that above 260 GPa, the Raman signal disappears and the resistivity of the sample drops drastically. However, immediately after this report, it was found that hydrogen exists in a mixed atomic and molecular semiconducting solid phase (IV) at least up

*pchem.neetik@gmail.com

†chandra@barc.gov.in

‡Corresponding author: akroy@iiserkol.ac.in; akroy6k@gmail.com

to 315 GPa at 300 °K [17]. Moreover, at lower temperature, phase IV transforms to phase III [18]. Additionally, it was also established that the Raman signal is lost due to a loss of hydrogen. The sample resistance drops due to chamber collapse [19]. However, these studies have provided the required insight about the $P - T$ condition to convert the molecular gas into a monatomic metal. A new phase (V) of hydrogen has been observed experimentally in room temperature under 325 GPa [20]. Recently, the insulator to metal transition in liquid deuterium has been observed experimentally (at around 400 GPa and 1000 °K) using the shock-wave technology [21,22]. Thus it seems that at a high pressure regime, a plethora of interesting and exciting properties are observed in hydrogen, but the metallic state at low temperature remains elusive. In the present attempt, we would like to investigate metal-like properties in H-like ions and plasmas under high pressure using the *Herzfeld criterion* of polarizability [23].

The simplest plasma condition is introduced by invoking the Debye-Hückel potential (DP). In the last two decades, DP was investigated vigorously with the utmost attention. For example, the effect of plasma screening on the energy spectrum [24–27], virial and Hellmann-Feynman theorem [28], two 4-proton transitions [29,30], transition probabilities connecting electron-impact excitation [31–33], inelastic electron-ion scattering [34,35], Fisher information, Shannon entropy, statistical complexity [36], etc., have been studied. Numerical values of the critical screening constant $\lambda^{(c)}$ for ground and low-lying excited states were presented in [37]. Recently, an empirical relation between $\lambda_{n,\ell}^{(c)}$ and Z was proposed in [38]. Spectroscopic properties, together with multipole oscillator strength (OS) and static multipole polarizabilities, were evaluated [39–43] using various numerical methods.

The exponential cosine screened Coulomb potential (ECSCP) exerts a stronger effect compared to DP. The existence of the oscillatory part manifests in a combined screening and wake effect around a slow-moving test charge in high plasma number density (n_e), low T plasma. The cosine term drives the quantum force enacting on plasma electrons to predominate over statistical pressure exerted by plasmas [44,45]. In quantum plasma, λ_D depends on the wave number of the electron. Its eigenvalue and eigenfunctions were studied using various quantum-chemical methods [46–56]. The influence of λ_D on the energy spectrum [26,27], photoionization cross section [51,57], electron-impact excitation [33], etc., has been probed as well. Similar to DP, an attempt was made to determine the characteristic λ_D beyond which the bound states cease to exist [38,58]. The laser-induced excitation on the confined H atom (CHA) in ECSCP was reported in terms of laser pulse, r_c , λ_D using the Bernstein polynomial [59]. Variations of $f^{(1)}$, $\alpha^{(1)}$ against λ_D were reported in [45,48,49,55,56,60]. In ion-sphere plasmas (ISPs), plasmalike behavior is observed within the ion sphere of radius R . Inside that radius, plasma electrons are uniformly distributed [61,62]. The energy spectrum, spectroscopic properties such as static polarizabilities, photoionization cross section, etc. of ISPs have been investigated by using several theoretical procedures [63–65].

In chemistry, the shell-confinement condition can be illustrated by citing the examples of trapping of an atom

or molecule within the *metal organic framework* [66,67], inside the fullerene cage, and zeolite cavity [68]. The sintering effect gets minimized; as a consequence, the catalytic activity and thermal stability of certain *noble* metals are improved [67,69–72]. Further, such a condition amplifies the photoluminescence character in nanocrystals by reducing nonradiative Auger processes [66,73] and dispels defects in polymer crystals [74,75], etc. Shell confinement plays a key role in energy storage [76–78], therapeutics [79], and pollution control [80,81]. A recent theoretical study also reveals that with increase in pressure, the $(H_2)_n$ clusters trapped inside the endohedral cavity become dominantly atomic [82]. Therefore, it will be interesting to investigate the metal-like behavior of hydrogen under such stressed chemical environment.

In 1927, Herzfeld defined a criterion of metallization while answering the question “when will an element show metallic conductivity?” He suggested that under a stressed condition, metallic behavior prevails, if dipole polarizability $\alpha^{(1)}$ of the system becomes greater than its volume (V). In this context, he also pointed out that this relation is valid for monatomic vapor, nearly cubic (simple) solids, and monatomic liquids [23]. This was pursued to examine the metal-like character in the $1s$ state of a *shell-confined* H atom or H-like ions (SCHA). Further, according to the Herzfeld criterion (HC), such phenomena can only be observed in s waves (not in $\ell \neq 0$ states) involving SCHA [83]. Moreover, in confined H-like ions (CHA), $\alpha^{(1)}$ is always less than V . In this endeavor, our objective is threefold. First of all, we intend to apply the existing HC for several hydrogenic plasmas such as DP, ECSCP, and ISP. Later, we would like to remodel HC in terms of the pressure of the system. This can be achieved by replacing V with pressure in HC. In principle, this will provide us with an immediate alternative to measure the metal-like pattern in atoms or plasmas under high pressure. It is a well known fact that the metallic character in hydrogen is observed at very high temperature and pressure. Therefore, the system is obviously not in its ground state [2,21,22]. Moreover, at a given pressure, V is the same for all elements (as it is chosen to be the volume of the vessel). However, actually, both the pressure and volume alter with the change in state as well as system. It means that these two quantities depend on the nuclear charge (Z), screening constant (λ), as well as quantum numbers n, ℓ . Therefore, we have to incorporate the environmental effect in HC by invoking several scaling ideas. The present modified form of HC incorporates the influence of all the parameters present in the Hamiltonian. The utility and efficiency of this expression is examined for CHA, SCHA, DP, ECSCP, and ISP. Finally, on the basis of the HC, we have commented about the metal-like character of the H atom and plasmas trapped inside a fullerene moiety. This article is planned as follows: Sec. II provides a detailed description of the formalism employed in the present work. Section III offers a detailed discussion of the results. Finally, we conclude with a few remarks in Sec. IV.

II. THEORETICAL FORMALISM

The time-independent nonrelativistic radial Schrödinger equation (SE) in the *shell-confined condition* is expressed as

(in atomic units)

$$\left\{ -\frac{1}{2} \frac{d^2}{dr^2} + \frac{\ell(\ell+1)}{2r^2} + v(r) + V_0[1 - \theta(r - R_a) + \theta(r - R_b)] \right\} \psi_{n,\ell}(r) = \mathcal{E}_{n,\ell} \psi_{n,\ell}(r), \quad (1)$$

where $v(r)$ is the potential under confinement. Our desired situation can be envisaged by invoking the term $V_0[1 - \theta(r - R_a) + \theta(r - R_b)]$, with V_0 representing a large number that approaches ∞ . The *Heaviside theta functions*, $\theta(r - R_a)$, $\theta(r - R_b)$, become *unity* at $r \geq R_a$ and $r \geq R_b$, and zero otherwise. Also, $f[r] = [1 - \theta(r - R_a)]$ vanishes at $r \geq R_a$ and 1 at $r < R_a$. Besides this model, one can also make use of the following to describe the situation:

$$\left[-\frac{1}{2} \frac{d^2}{dr^2} + \frac{\ell(\ell+1)}{2r^2} + v(r) + \left(\frac{R_a}{r}\right)^k + \left(\frac{r}{R_b}\right)^k \right] \psi_{n,\ell}(r) = \mathcal{E}_{n,\ell} \psi_{n,\ell}(r). \quad (2)$$

At $k \rightarrow \infty$, $(\frac{R_a}{r})^k$ approaches ∞ in the $r \leq R_a$ region and becomes zero at $r > R_a$. On the contrary, $(\frac{r}{R_b})^k$ climbs up to ∞ at $r \geq R_b$, and zero otherwise. In essence, the potential $v(r)$ becomes effective in the range at $R_a \leq r \leq R_b$. It is noteworthy to mention that at $R_a = 0$ and $R_b = R$, both of these models reduce to a conventional hard confinement model. In the present work, all numerical calculations are performed using Eq. (1).

Another prototypical example of shell confinement is the trapping of an atom or molecule inside a fullerene cavity and zeolite cage or within a metal-organic framework. The corresponding radial SE under high pressure is conveniently expressed as [84–87]

$$\left[-\frac{1}{2} \frac{d^2}{dr^2} + \frac{\ell(\ell+1)}{2r^2} + v(r) + v_c(r) + v_R(r) \right] \psi_{n,\ell}(r) = \mathcal{E}_{n,\ell} \psi_{n,\ell}(r),$$

$$v_c(r) = \frac{V_1}{1 + \exp\left[-\left(\frac{r-(R_0+\Delta)}{\gamma}\right)\right]} - \frac{V_1}{1 + \exp\left[-\left(\frac{r-R_0}{\gamma}\right)\right]}. \quad (3)$$

Here, $v_R(r)$ can be chosen as $v_R(r) = (\frac{r}{R})^k$ or $v_R(r) = V_0\theta(r - R)$.

In the above equation, R_0 is the inner radius of the cavity with thickness Δ , and V_1 is the well depth with γ the smoothing parameter. Further, one can also change the electronic configuration by modulating V_1 [87]. Under ambient pressure (1 atm), the experimental values are $V_1 = 0.302$ a.u., $R_0 = 5.8$ a.u., $\Delta = 1.89$ a.u., and $\gamma = 0.1$ a.u. [85,88,89]. However, in the present case, we have assumed that these values remain unaltered with a change in pressure.

The plasma potentials are expressed in the following generalized form [63]:

$$v(r) = -\frac{Z}{r}(1 + br)e^{-\lambda r} \cos(c\lambda r), \quad (4)$$

where b, c, λ are positive real numbers. Depending upon the values of these two parameters, Eq. (4) modifies to three undermentioned forms:

$$(1) \ b = \lambda = c = 0, \text{ the H-like ions: } v(r) = -\frac{Z}{r}.$$

(2) $b = c = 0, \lambda \geq 0$, the Debye-Hückel potential [90]:

$v(r) = -\frac{Z}{r}e^{-\lambda_1 r}$. The Debye radius is $D = \frac{1}{\lambda_1} = \sqrt{\frac{k_B T_e}{4\pi e^2 n_e}}$. In DP, the probability of finding plasma particles within the Debye sphere is negligible. In the free condition, there arises the plasma-tail effect due to the presence of the asymptotic part in the plasma potential. With an increase in T_e , the charge cloud gets diffused, leading to an enhancement of this effect, which declines with an increase in external pressure [38]. In the confined condition, it is assumed that the charge cloud remains inside the spherical enclosure.

(3) $b = 0, c = 1, \lambda \geq 0$, the ECSCP [91]: $v(r) = -\frac{Z}{r}e^{-\lambda_2 r} \cos(\lambda_2 r)$. Here, D approaches the de Broglie wavelength; as a consequence, the quantum effect appears and λ_2 is connected to the plasma frequency through $\lambda_2 = \sqrt{\omega_{pe}}$. Further, a multiparticle cooperative interaction is enhanced with an increase in ion density. The presence of an additional *cosine* term provides a stronger screening effect compared to DP.

Besides these, the ISP model is explained as [92]

$$v_{\text{ISP}}(r) = \begin{cases} -\frac{Z}{r} + \left(\frac{Z-N_e}{2R}\right)\left[3 - \left(\frac{r}{R}\right)^2\right] & r \leq R \\ 0, & r > R. \end{cases} \quad (5)$$

In this case, the ion is trapped inside a spherically symmetric enclosure with radius R . Beyond R , the effect of the potential vanishes. Such plasmas are experimentally designed in a laboratory environment using a laser pulse. Now the radial SE becomes

$$\left[-\frac{1}{2} \frac{d^2}{dr^2} + \frac{\ell(\ell+1)}{2r^2} + v_{\text{ISP}}(r) + v_0 \theta(r - R) \right] \psi_{n,\ell}(r) = \mathcal{E}_{n,\ell} \psi_{n,\ell}(r). \quad (6)$$

Systems having $R_a = 0$ and $R_b = R$ will be referred to as confined systems. For numerical purposes, we invoke the generalized pseudospectral (GPS) method to evaluate energies, dipole oscillator strength, and polarizability. The utility and efficiency of this method in both *free* and *confined* conditions has been well documented in [93–100].

A. Shell-confined plasmas

High energy-density physics covers a broad range of plasmas from very hot to dense conditions. In this scenario, there occurs a coupling between plasma electrons and immersed atoms, leading to a change in electronic properties. The composite influences of plasma free-electron density (n_e) and temperature (T) play a crucial role in stabilizing a bound state by controlling the strength of this coupling represented through a coupling parameter (Γ) defined as below [38,63,101],

$$\Gamma = \frac{r_-}{a} = \frac{E_{\text{Coulomb}}}{E_{\text{thermal}}} = \frac{Q^2}{aT}, \quad (7)$$

where r_- is the critical radius of a circular volume beyond which no plasma electron can approach the atom [63], $a = (\frac{3}{4\pi n_e})^{\frac{1}{3}}$ is the interparticle spacing, called *ion-sphere radius*, and Q denotes the charge of the ion. $\Gamma \ll 1$ signifies a high T , low n_e condition (weakly coupled), while, $\Gamma \gg 1$ represents a low T , high n_e situation (strongly coupled). In

a given plasma, the correlated many-particle interactions are described by an average screening potential, incorporating the collective effects due to the presence of a charged cloud [87]. In a dense plasma, the competing effects of n_e and T are modulated through the Debye length, $\lambda_D = (\frac{T}{4\pi Q^2 n_e})^{\frac{1}{2}}$. At high T and low n_e , λ_D possesses a higher value and, as a consequence, offers a greater number of bound states. On the contrary, λ_D decreases at low T and high n_e , leading to a decrease in the count of bound states. Further, the plasma-tail effect appears in the picture as T rises.

In plasmas, the atom or ion is encompassed by (+)ve/(-)ve mobile charges. The relative density of the surrounding particles is measured through the radial distribution function $g(r)$. It is ubiquitous in plasmas and is expressed as [63]

$$g(r) = \left[1 - \frac{Q}{T_e} \phi(r) \right]. \quad (8)$$

Here, Q is the charge and T_e refers to plasma temperature; $\phi(r)$ signifies the solution of the Poisson-Boltzmann equation. For DP and ECSCP, Eq. (8) leads to

$$g(r) = \left[1 - \frac{Q}{T_e r} e^{-\lambda r} \right] \text{ for DP,}$$

$$g(r) = \left[1 - \frac{Q}{T_e r} e^{-\lambda r} \cos \lambda r \right] \text{ for ECSCP.} \quad (9)$$

Equation (9) suggests that in either of the plasmas at $r \rightarrow 0$, $g(r)$ becomes (-)ve. This is an unphysical condition, as all particles repel each other. In order to gain stability, it becomes a forbidden region for the particle. This no-go zone is called *ion sphere* with radius a . Physically, $g(r) \rightarrow 0$ at $r \rightarrow a$. This situation is appropriately explained by adopting the *shell-confined* model, as it can efficiently explain this limiting criterion. Further, by modulating R_b , we can meet the condition $g(r) \rightarrow 1$ at large r . Moreover, this change in R_b also incorporates the temperature effect. The plasma-tail effect [38] predominates with a rise in R_b . However, ISP is beyond the scope of the shell-confined model because, in this case, the central charged ion is trapped inside the pool of charged particle within the ion sphere. Therefore, at the said forbidden region, $g(r)$ becomes finite.

B. Dipole polarizability and HC of metallization

The static dipole polarizability is expressed as

$$\alpha_{nl}^{(1)} = \alpha_{nl}^{(1)}(\text{bound}) + \alpha_{nl}^{(1)}(\text{continuum}), \quad (10)$$

where the first and second terms represent bound and continuum contributions (the selection rule for the dipole transition is $\Delta\ell = \pm 1$). From perturbation theory consideration, these may be expressed as [92,102]

$$\alpha_{nl}^{(1)}(\text{bound}) = \sum_i \left[\frac{f_{nl \rightarrow i(\ell-1)}^{(1)}}{(\mathcal{E}_{i(\ell-1)} - \mathcal{E}_{nl})^2} + \frac{f_{nl \rightarrow i(\ell+1)}^{(1)}}{(\mathcal{E}_{i(\ell+1)} - \mathcal{E}_{nl})^2} \right],$$

$$\alpha_{nl}^{(1)}(\text{continuum}) = c \int \frac{| \langle R_{nl} | r Y_{kq}(\mathbf{r}) | R_{ep} \rangle |^2}{(\mathcal{E}_{ep} - \mathcal{E}_{nl})} d\epsilon. \quad (11)$$

The analytical closed-form expression of the dipole oscillator strength, $f_{nl \rightarrow n'\ell'}^{(1)}$, can be written as

$$f_{nl \rightarrow n'\ell'}^{(1)} = \frac{2}{3} (2\ell' + 1) (\mathcal{E}_{n'\ell'} - \mathcal{E}_{nl}) |\langle r \rangle_{nl}^{n'\ell'}|^2 \begin{Bmatrix} \ell' & 1 & \ell \\ 0 & 0 & 0 \end{Bmatrix}^2. \quad (12)$$

The transition matrix element is evaluated using the following radial integral:

$$\langle r \rangle_{nl}^{n'\ell'} = \int_0^\infty R_{n'\ell'}(r) r R_{nl}(r) r^2 dr. \quad (13)$$

The dipole oscillator strength sum rule is stated as

$$S_{nl}^{(1)} = \sum_j f_{nl \rightarrow j\ell'}^{(1)} = \langle \psi_{nl} | \psi_{nl} \rangle = 1, \quad (14)$$

where the summation includes the contribution from both bound and continuum states (j), whereas ℓ' signifies both the $(\ell + 1)$ and $(\ell - 1)$ states.

According to HC [23], the insulator to metallic conversion occurs after attaining a threshold value of $\alpha_{nl}^{(1)}$ having the form

$$V \leq \frac{4}{3} \pi \alpha_{nl}^{(1)}, \quad \chi_m = \frac{\alpha_{nl}^{(1)}}{V} \geq \frac{3}{4\pi}. \quad (15)$$

Here, V signifies the closed volume under which an atom or ion is trapped. This relation is valid for monatomic vapor, nearly cubic (simple) solids, and monatomic liquids [23]. The ratio $\frac{\alpha_{nl}^{(1)}}{V} = \chi_m$ (subscript m signifies metal) can act as an indicator of metallization. Thus, one can easily conclude that $\chi_m \geq \frac{3}{4\pi}$ for metals and $\chi_m < \frac{3}{4\pi}$ for nonmetals. Therefore, we define χ_m as a descriptor of the metallic character in an atom or ion. This provides a lower bound of χ_m , while $\alpha_{nl}^{(1)}$ is a state-dependent quantity, but χ_m is a universal descriptor. This lower bound can be further modified to unity. Depending upon the nature of confinement, the following situations may arise:

(1) For a *spherically* confined atom, since $V = \frac{4}{3} \pi R^3$, Eq. (15) gives

$$\chi_m = \frac{\alpha_{nl}^{(1)}}{R^3} \geq 1. \quad (16)$$

(2) For a *shell-confined* atom, since $V = \frac{4}{3} \pi (R_b^3 - R_a^3)$, Eq. (15) can be recast to

$$\chi_m = \frac{\alpha_{nl}^{(1)}}{(R_b^3 - R_a^3)} \geq 1. \quad (17)$$

Thus it appears that one can follow the metallic behavior in confined atomic systems, in terms of χ_m becoming greater than or equal to unity. This criterion was used to examine the metallic character in atomic H and plasmas. It was reported for s -wave states in a *shell-confined* H atom. But for $\ell \neq 0$ states, it is always less than unity [83,103]. Further, for confined systems, χ_m never crosses the threshold mark. But, some literature suggests that the metallic character could be observed at extreme pressure, when the system is in an excited state [2,21,22]. In this regard, we shall first try to recast Eq. (15) in terms of pressure (P_{nl}). Second, it would be useful to incorporate the environmental contributions by envisaging the effect of Z , λ , R_a , R_b in χ_m .

At the onset, we would like to replace V in Eq. (15) in terms of $P_{n,\ell}$. The thermodynamic equation of state suggests that under an *adiabatic* environment, $P_{n,\ell}$ can be written as $P_{n,\ell} = -\left(\frac{\partial \mathcal{E}_{n,\ell}}{\partial V}\right)$. In confined systems, it (a state-dependent property) can be expressed in the following form [104,105]:

$$P_{n,\ell} = -\left(\frac{\partial \mathcal{E}_{n,\ell}}{\partial V}\right) = -\left(\frac{\partial \mathcal{E}_{n,\ell}}{\partial R}\right)\left(\frac{\partial R}{\partial V}\right). \quad (18)$$

Further, using Eqs. (16), one can write $\frac{\partial V}{\partial R} = \frac{3V}{R}$. Therefore, the following situation can be envisaged:

$$3VP_{n,\ell} = -R\left(\frac{\partial \mathcal{E}_{n,\ell}}{\partial R}\right). \quad (19)$$

Now replacing V in Eq. (15), one finally achieves the following form:

$$P_{n,\ell}\alpha_{n\ell}^{(1)} \geq -\frac{3R}{4\pi}\left(\frac{\partial \mathcal{E}_{n,\ell}}{\partial R}\right). \quad (20)$$

Let us define $\zeta_{n,\ell} = P_{n,\ell}\alpha_{n\ell}^{(1)}$. The above relation suggests that in an atom, the metallic nature may be observed when $\zeta_{n\ell}$ predominates over the corresponding right-hand side quantity presented in Eqs. (20), respectively. It is worth mentioning that in either atom, the right- and left-hand sides become *state dependent*. An increase in R always leads to a decrease in $P_{n,\ell}$; therefore, $\mathcal{E}_{n,\ell}$ declines with a reduction of $P_{n,\ell}$. As a consequence, $\frac{\partial \mathcal{E}_{n,\ell}}{\partial R}$ becomes *negative*. Hence, the right-hand side of Eqs. (20) always remains *positive*. At a given λ , the expression of $P_{n,\ell}$ in Eq. (18) is valid for both plasmas. Unfortunately, the analytical closed-form expressions of $\left(\frac{\partial \mathcal{E}_{n,\ell}}{\partial R}\right)$ for DP, ECSCP, etc. in both confined and shell-confined systems are not yet known. In future works, we may engage into such relations. However, we concentrate on modifying χ_m .

C. Scaling concept

In plasma potentials, the scaling concept has been discussed previously in [28,38,64,92,106]. However, so far the scaling concept has not been extended to a *shell-confined* quantum system, which we pursue here. Thus, starting from an arbitrary set of Z, λ, R_a, R_b , one can derive four independent scaling ideas. We attempt to connect all these ideas into a single equation. Thus one can estimate a given desired property for a series of Z, λ, R_a, R_b , related by the scaling concepts. To proceed further, we have used Eq. (1) to derive the required scaling relations. However, similar relations can also be extracted by employing Eq. (2). To move forward, we write Eq. (1) as

$$\left\{-\frac{\hbar}{2m}\nabla^2 + V(r, Z, \lambda, R_a, R_b) + V_0[1 - \theta(r - R_a) + \theta(r - R_b)]\right\}\psi_{n,\ell}(r) = \mathcal{E}_{n,\ell}\psi_{n,\ell}(r). \quad (21)$$

In the above, $v(r, Z, \lambda, R_a, R_b)$ is the Coulombic potential, where Z, λ both appear in the *linear* part. Now we derive analytical relations among $f_{n\ell}^{(k)}, \alpha_{n\ell}^{(k)}, \mathcal{E}_{n,\ell}$ in terms of $Z, \lambda, R_a,$

and R_b . In this context, four independent and parallel scaling concepts will be employed. Using atomic units, we have $\hbar = m = 1$.

(1) Applying a transformation ($r = Zr_1$), the Hamiltonian can be modified as

$$H(Z; \lambda; R_a, R_b; r) \leftrightarrow H\left(1; \frac{\lambda}{Z}; ZR_a, ZR_b; r_1\right). \quad (22)$$

Thus, the Z -containing part becomes free from it. By taking that into account, the radial SE can be written as

$$\left\{-\frac{1}{2}\nabla_1^2 + V\left(r_1, 1, \frac{\lambda}{Z}, ZR_a, ZR_b\right) + Z^2V_0[1 - \theta(r_1 - ZR_a) + \theta(r_1 - ZR_b)]\right\}\psi_{n,\ell}(r_1) = Z^2\mathcal{E}_{n,\ell}\left(1, \frac{\lambda}{Z}, ZR_a, ZR_b\right)\psi_{n,\ell}(r_1). \quad (23)$$

The $\psi_{n,\ell}(r)$, $\mathcal{E}_{n,\ell}$, $f_{n\ell}^{(k)}$, and $\alpha_{n\ell}^{(k)}$ of the initial and modified Hamiltonians are found to be connected as

$$\begin{aligned} \mathcal{E}_{n,\ell}(Z, \lambda, R_a, R_b) &= Z^2\mathcal{E}_{n,\ell}\left(1, \frac{\lambda}{Z}, ZR_a, ZR_b\right), \\ \psi_{n,\ell}(Z; \lambda; R_a, R_b; r) &= \frac{1}{Z^{\frac{3}{2}}}\psi_{n,\ell}\left(1; \frac{\lambda}{Z}; ZR_a, ZR_b; r_1\right), \\ f_{n\ell}^{(k)}(Z, \lambda, R_a, R_b) &= \frac{f_{n\ell}^{(k)}\left(1, \frac{\lambda}{Z}, ZR_a, ZR_b\right)}{Z^{2(k-1)}}, \\ \alpha_{n\ell}^{(k)}(Z, \lambda, R_a, R_b) &= \frac{\alpha_{n\ell}^{(k)}\left(1, \frac{\lambda}{Z}, ZR_a, ZR_b\right)}{Z^{2(k+1)}}. \end{aligned} \quad (24)$$

Equation (24) clearly indicates that $f_{n\ell}^{(1)}$ remains unaffected with Z scaling.

(2) Next, replacing $r = \frac{r_2}{\lambda}$, one can map the effective Hamiltonian as

$$H(Z; \lambda; R_a, R_b; r) \leftrightarrow H\left(\frac{Z}{\lambda}; 1; \lambda R_a, \lambda R_b; r_2\right). \quad (25)$$

In this occasion, the λ -containing part becomes independent. The SE now becomes

$$\left\{-\frac{1}{2}\nabla_2^2 + V\left(r_2, \frac{Z}{\lambda}, 1, \lambda R_a, \lambda R_b\right) + \frac{1}{\lambda^2}V_0[1 - \theta(r_2 - \lambda R_a) + \theta(r_2 - \lambda R_b)]\right\}\psi_{n,\ell}(r_2) = \lambda^2\mathcal{E}_{n,\ell}\left(\frac{Z}{\lambda}, 1, \lambda R_a, \lambda R_b\right)\psi_{n,\ell}(r_2). \quad (26)$$

The quantities from the initial and modified Hamiltonians are seen to be related as

$$\begin{aligned} \mathcal{E}_{n,\ell}(Z, \lambda, R_a, R_b) &= \lambda^2\mathcal{E}_{n,\ell}\left(\frac{Z}{\lambda}, 1, \lambda R_a, \lambda R_b\right), \\ \psi_{n,\ell}(Z; \lambda; R_a, R_b; r) &= \lambda^{\frac{3}{2}}\psi_{n,\ell}\left(\frac{Z}{\lambda}; 1; \lambda R_a; \lambda R_b; r_2\right), \\ f_{n\ell}^{(k)}(Z, \lambda, R_a, R_b) &= \frac{f_{n\ell}^{(k)}\left(\frac{Z}{\lambda}, 1, \lambda R_a, \lambda R_b\right)}{\lambda^{2(k-1)}}, \\ \alpha_{n\ell}^{(k)}(Z, \lambda, R_a, R_b) &= \frac{\alpha_{n\ell}^{(k)}\left(\frac{Z}{\lambda}, 1, \lambda R_a, \lambda R_b\right)}{\lambda^{2(k+1)}}. \end{aligned} \quad (27)$$

As usual, $f_{nl}^{(1)}$ remains unchanged with λ scaling.

(3) Substituting $r = R_a r_3$, one can write the Hamiltonian in the form below,

$$H(Z; \lambda; R_a, R_b; r) \leftrightarrow H\left(ZR_a; \lambda R_a; 1; \left[\frac{R_b}{R_a}\right]; r_3\right). \quad (28)$$

Hence R_a is fixed at 1. Therefore, the SE converts to the given form,

$$\begin{aligned} & -\frac{1}{2}\nabla_3^2\psi_{n,\ell}(r_3) + V\left(r_3, ZR_a, \lambda R_a, 1, \left[\frac{R_b}{R_a}\right]\right)\psi_{n,\ell}(r_3) \\ & + R_a^2 V_0[1 - \theta(r_3 - 1)]\psi_{n,\ell}(r_3) \\ & + R_a^2 V_0\left\{\theta\left(r_3 - \left[\frac{R_b}{R_a}\right]\right)\right\}\psi_{n,\ell}(r_3) \\ & = R_a^2 \mathcal{E}_{n,\ell}\left(ZR_a, \lambda R_a, 1, \left[\frac{R_b}{R_a}\right]\right)\psi_{n,\ell}(r_3). \end{aligned} \quad (29)$$

Thus, $\psi_{n,\ell}(r)$, $\mathcal{E}_{n,\ell}$, $f_{nl}^{(k)}$, and $\alpha_{nl}^{(k)}$ of the initial and modified Hamiltonians are connected as

$$\begin{aligned} \mathcal{E}_{n,\ell}(Z, \lambda, R_a, R_b) &= R_a^2 \mathcal{E}_{n,\ell}\left(ZR_a, \lambda R_a, 1, \left[\frac{R_b}{R_a}\right]\right), \\ \psi_{n,\ell}(Z; \lambda; R_a, R_b; r) &= \frac{1}{R_a^{\frac{3}{2}}}\psi_{n,\ell}\left(ZR_a; \lambda R_a, 1, \left[\frac{R_b}{R_a}\right]; r_3\right), \\ f_{nl}^{(k)}(Z, \lambda, R_a, R_b) &= \frac{f_{nl}^{(k)}\left(ZR_a, \lambda R_a, 1, \left[\frac{R_b}{R_a}\right]\right)}{R_a^{2(k-1)}}, \\ \alpha_{nl}^{(k)}(Z, \lambda, R_a, R_b) &= \frac{\alpha_{nl}^{(k)}\left(ZR_a, \lambda R_a, 1, \left[\frac{R_b}{R_a}\right]\right)}{R_a^{2(k+1)}}. \end{aligned} \quad (30)$$

Equation (30) suggests $f_{nl}^{(1)}$ remains invariant with R_a scaling.

(4) Replacing $r = R_b r_4$, one can transform the Hamiltonian in the form given below,

$$H(Z; \lambda; R_a, R_b; r) \leftrightarrow H\left(ZR_b; \lambda R_b; \left[\frac{R_a}{R_b}\right], 1; r_4\right). \quad (31)$$

Thus, R_b is fixed at 1. Further, we get $\left(\frac{R_a}{R_b}\right) < 1$. The SE now transforms to the form given below,

$$\begin{aligned} & -\frac{1}{2}\nabla_4^2\psi_{n,\ell}(r_4) + V\left(r_4, ZR_b, \lambda R_b, \left[\frac{R_a}{R_b}\right], 1\right)\psi_{n,\ell}(r_4) \\ & + R_b^2 V_0[\theta(r_4 - 1)]\psi_{n,\ell}(r_4) \\ & + R_b^2 V_0\left\{1 - \theta\left(r_4 - \left[\frac{R_a}{R_b}\right]\right)\right\}\psi_{n,\ell}(r_4) \\ & = R_b^2 \mathcal{E}_{n,\ell}\left(ZR_b, \lambda R_b, \left[\frac{R_a}{R_b}\right], 1\right)\psi_{n,\ell}(r_4). \end{aligned} \quad (32)$$

The desired quantities in the initial and modified Hamiltonians are related as

$$\begin{aligned} \mathcal{E}_{n,\ell}(Z, \lambda, R_a, R_b) &= R_b^2 \mathcal{E}_{n,\ell}\left(ZR_b, \lambda R_b, \left[\frac{R_a}{R_b}\right], 1\right), \\ \psi_{n,\ell}(Z; \lambda; R_a, R_b; r) &= \frac{1}{R_b^{\frac{3}{2}}}\psi_{n,\ell}\left(ZR_b; \lambda R_b, \left[\frac{R_a}{R_b}\right], 1; r_4\right), \end{aligned}$$

$$f_{nl}^{(k)}([Z, \lambda, R_a, R_b]) = \frac{f_{nl}^{(k)}\left(ZR_b, \lambda R_b, \left[\frac{R_a}{R_b}\right], 1\right)}{R_b^{2(k-1)}},$$

$$\alpha_{nl}^{(k)}(Z, \lambda, R_a, R_b) = \frac{\alpha_{nl}^{(k)}\left(ZR_b, \lambda R_b, \left[\frac{R_a}{R_b}\right], 1\right)}{R_b^{2(k+1)}}. \quad (33)$$

Equation (33) suggests that $f_{nl}^{(1)}$ remains unaltered with R_b scaling.

Thus, as can be seen, we have converted the initial Hamiltonian, given by Eq. (1), into four independent scaled Hamiltonians, viz., Eqs. (23), (26), (29), and (32). Now combining Eqs. (24), (27), (30), and (33), one can write the unified equation for $\mathcal{E}_{n,\ell}$,

$$\begin{aligned} \mathcal{E}_{n,\ell}(Z, \lambda, R_a, R_b) &= Z^2 \mathcal{E}_{n,\ell}\left(1, \frac{\lambda}{Z}, ZR_a, ZR_b\right) \\ &= \lambda^2 \mathcal{E}_{n,\ell}\left(\frac{Z}{\lambda}, 1, \lambda R_a, \lambda R_b\right) \\ &= R_a^2 \mathcal{E}_{n,\ell}\left(ZR_a, \lambda R_a, 1, \left[\frac{R_b}{R_a}\right]\right) \\ &= R_b^2 \mathcal{E}_{n,\ell}\left(ZR_b, \lambda R_b, \left[\frac{R_a}{R_b}\right], 1\right), \end{aligned} \quad (34)$$

$$\begin{aligned} f_{nl}^{(k)}(Z, \lambda, R_a, R_b) &= \frac{f_{nl}^{(k)}\left(1, \frac{\lambda}{Z}, ZR_a, ZR_b\right)}{Z^{2(k-1)}} \\ &= \frac{f_{nl}^{(k)}\left(\frac{Z}{\lambda}, 1, \lambda R_a, \lambda R_b\right)}{\lambda^{2(k-1)}} \\ &= \frac{f_{nl}^{(k)}\left(ZR_a, \lambda R_a, 1, \left[\frac{R_b}{R_a}\right]\right)}{R_a^{2(k-1)}} \\ &= \frac{f_{nl}^{(k)}\left(ZR_b, \lambda R_b, \left[\frac{R_a}{R_b}\right], 1\right)}{R_b^{2(k-1)}}, \end{aligned} \quad (35)$$

$$\begin{aligned} \alpha_{nl}^{(k)}(Z, \lambda, R_a, R_b) &= \frac{\alpha_{nl}^{(k)}\left(1, \frac{\lambda}{Z}, ZR_a, ZR_b\right)}{Z^{2(k+1)}} \\ &= \frac{\alpha_{nl}^{(k)}\left(\frac{Z}{\lambda}, 1, \lambda R_a, \lambda R_b\right)}{\lambda^{2(k+1)}} \\ &= \frac{\alpha_{nl}^{(k)}\left(ZR_a, \lambda R_a, 1, \left[\frac{R_b}{R_a}\right]\right)}{R_a^{2(k+1)}} \\ &= \frac{\alpha_{nl}^{(k)}\left(ZR_b, \lambda R_b, \left[\frac{R_a}{R_b}\right], 1\right)}{R_b^{2(k+1)}}. \end{aligned} \quad (36)$$

Figure 1 now pictorially represents the interconversion framework. It indicates that performing the calculation at a definite set of (Z, λ, R_a, R_b) , one can estimate the properties of other sets of Z, λ, R_a, R_b (connected by scaling) without solving the SE. These are derived for any four-parameter potentials. In DP and ECSCP, λ becomes λ_1, λ_2 , respectively.

D. Descriptor of metallization

The volume of a quantum system is entirely controlled by its state as well as environment. But here V is a function of R only. As a consequence, Eqs. (15) to (17) do not comment about the influence of Z, λ , and the boundary condition (R_a, R_b) on χ_m . Therefore, it is necessary to introduce the

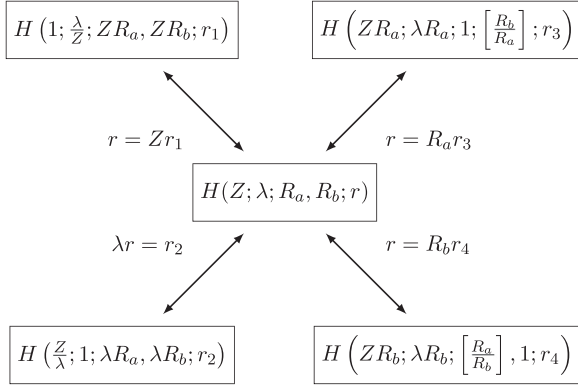


FIG. 1. Schematic diagram to describe the interconversion among five Hamiltonians through scaling transformation. See text for details.

effect of surrounding by assimilating all these parameters in the expression of χ . In the future, this modification can be treated as an environmental correction on it. Before going into the detailed derivation, it should be kept in mind that HC is applicable for all monatomic vapors. Therefore, χ_m obtained from all four Hamiltonians discussed in Sec. II C and Fig. 1 must be greater than or equal to unity.

Now invoking Eq. (24) and putting $k = 1$, one obtains

$$\begin{aligned}\alpha_{n\ell}^{(1)}(Z, \lambda, R_a, R_b) &= \frac{\alpha_{n\ell}^{(1)}\left(1, \frac{\lambda}{Z}, ZR_a, ZR_b\right)}{Z^4}, \\ \frac{\alpha_{n\ell}^{(1)}(Z, \lambda, R_a, R_b)}{(R_b^3 - R_a^3)} &= \frac{\alpha_{n\ell}^{(1)}\left(1, \frac{\lambda}{Z}, ZR_a, ZR_b\right)}{Z^4(R_b^3 - R_a^3)}, \\ \chi_m(Z, \lambda, R_a, R_b) &= \frac{\chi_m\left(1, \frac{\lambda}{Z}, ZR_a, ZR_b\right)}{Z}, \\ Z \chi_m(Z, \lambda, R_a, R_b) &= \chi_m\left(1, \frac{\lambda}{Z}, ZR_a, ZR_b\right).\end{aligned}\quad (37)$$

Now, recalling the condition of metallization given in Eq. (15), one may write $\chi_m\left(1, \frac{\lambda}{Z}, ZR_a, ZR_b\right) \geq 1$.

Next, substituting $k = 1$ in Eq. (27), we get

$$\begin{aligned}\alpha_{n\ell}^{(1)}(Z, \lambda, R_a, R_b) &= \frac{\alpha_{n\ell}^{(1)}\left(\frac{Z}{\lambda}, 1, \lambda R_a, \lambda R_b\right)}{\lambda^4}, \\ \frac{\alpha_{n\ell}^{(1)}(Z, \lambda, R_a, R_b)}{(R_b^3 - R_a^3)} &= \frac{\alpha_{n\ell}^{(1)}\left(\frac{Z}{\lambda}, 1, \lambda R_a, \lambda R_b\right)}{\lambda^4(R_b^3 - R_a^3)}, \\ \chi_m(Z, \lambda, R_a, R_b) &= \frac{\chi_m\left(\frac{Z}{\lambda}, 1, \lambda R_a, \lambda R_b\right)}{Z}, \\ \lambda \chi_m(Z, \lambda, R_a, R_b) &= \chi_m\left(\frac{Z}{\lambda}, 1, \lambda R_a, \lambda R_b\right).\end{aligned}\quad (38)$$

Now let us mention the condition discussed in Eq. (15) as $\chi_m\left(\frac{Z}{\lambda}, 1, \lambda R_a, \lambda R_b\right) \geq 1$.

So, referring Eqs. (30) and choosing $k = 1$, we get

$$\begin{aligned}\alpha_{n\ell}^{(1)}(Z, \lambda, R_a, R_b) &= \frac{\alpha_{n\ell}^{(1)}\left(ZR_a, \lambda R_a, 1, \left[\frac{R_b}{R_a}\right]\right)}{R_a^4}, \\ \frac{\alpha_{n\ell}^{(1)}(Z, \lambda, R_a, R_b)}{(R_b^3 - R_a^3)} &= \frac{\alpha_{n\ell}^{(1)}\left(ZR_a, \lambda R_a, 1, \left[\frac{R_b}{R_a}\right]\right)}{R_a^4\left(\frac{R_b^3}{R_a^3} - 1\right)},\end{aligned}$$

$$\chi_m(Z, \lambda, R_a, R_b) = \frac{\chi_m\left(ZR_a, \lambda R_a, 1, \left[\frac{R_b}{R_a}\right]\right)}{R_a},$$

$$R_a \chi_m(Z, \lambda, R_a, R_b) = \chi_m\left(ZR_a, \lambda R_a, 1, \left[\frac{R_b}{R_a}\right]\right), \quad (39)$$

again using the condition available in Eq. (15) as $\chi_m\left(ZR_a, \lambda R_a, 1, \left[\frac{R_b}{R_a}\right]\right) \geq 1$.

Finally, we use Eq. (33) and replace $k = 1$ to get the following equations:

$$\alpha_{n\ell}^{(1)}(Z, \lambda, R_a, R_b) = \frac{\alpha_{n\ell}^{(1)}\left(ZR_b, \lambda R_b, \left[\frac{R_a}{R_b}\right], 1\right)}{R_b^4},$$

$$\frac{\alpha_{n\ell}^{(1)}(Z, \lambda, R_a, R_b)}{(R_b^3 - R_a^3)} = \frac{\alpha_{n\ell}^{(1)}\left(ZR_b, \lambda R_b, \left[\frac{R_a}{R_b}\right], 1\right)}{R_b^4\left(1 - \frac{R_a^3}{R_b^3}\right)},$$

$$\chi_m(Z, \lambda, R_a, R_b) = \frac{\chi_m\left(ZR_b, \lambda R_b, \left[\frac{R_a}{R_b}\right], 1\right)}{R_b},$$

$$R_b \chi_m(Z, \lambda, R_a, R_b) = \chi_m\left(ZR_b, \lambda R_b, \left[\frac{R_a}{R_b}\right], 1\right). \quad (40)$$

Again, the same Eq. (15) takes the form $\chi_m\left(ZR_b, \lambda R_b, \left[\frac{R_a}{R_b}\right], 1\right) \geq 1$.

When $R_a = 0$ and $R_b = R$ [$\chi_m(ZR, \lambda R, 1) \geq 1$ from Eq. (15)], we get the following from Eq. (33):

$$R \chi_m(Z, \lambda, R) = \chi_m(ZR, \lambda R, 1). \quad (41)$$

Our desired expression of modified HC can be derived in two different ways, namely, by considering a *product* and *sum* of the χ_m 's, which are denoted by $\chi_m^{th}(P)$ and $\chi_m^{th}(S)$ in the following discussion. At first, we discuss $\chi_m^{th}(P)$, then $\chi_m^{th}(S)$ and, finally, a comparative analysis between the two has been provided.

(1) Product (P): multiplying Eqs. (37)–(40), one can write

$$(Z \times \lambda \times R_a \times R_b) [\chi_m(Z, \lambda, R_a, R_b)]^4 = K, \quad (42)$$

where

$$\begin{aligned}K &= \chi_m\left(1, \frac{\lambda}{Z}, ZR_a, ZR_b\right) \times \chi_m\left(\frac{Z}{\lambda}, 1, \lambda R_a, \lambda R_b\right) \\ &\times \chi_m\left(ZR_a, \lambda R_a, 1, \left[\frac{R_b}{R_a}\right]\right) \times \chi_m\left(ZR_b, \lambda R_b, \left[\frac{R_a}{R_b}\right], 1\right).\end{aligned}\quad (43)$$

Here, $K \geq 1$ because all four constituent terms are individually ≥ 1 . Applying this condition in Eq. (43), one can easily obtain

$$(Z \times \lambda \times R_a \times R_b) \times [\chi_m(Z, \lambda, R_a, R_b)]^4 \geq 1,$$

$$(Z \times \lambda \times R_a \times R_b)^{\frac{1}{4}} \times \chi_m(Z, \lambda, R_a, R_b) = \chi'_m \geq 1. \quad (44)$$

Thus, we have arrived at a modified expression of χ_m in the form of χ'_m without changing the threshold value (which is 1). This form explains the influence of Z, λ and boundary conditions on χ_m . Instead of using χ'_m , one may further recast this equation into the following form, where the right-hand side becomes dependent on Z, λ, R_a, R_b :

$$\chi_m(Z, \lambda, R_a, R_b) \geq \chi_m^{th}(P) = \frac{1}{(Z \times \lambda \times R_a \times R_b)^{\frac{1}{4}}}. \quad (45)$$

Here, $\chi_m^{th}(P)$ signifies the threshold value of $\chi_m(Z, \lambda, R_a, R_b)$, beyond which metallization can be observed. This threshold value changes from one system to another. This criterion may be applied to ionic systems. Note that $R_a = 0$ and $R_b = R$, and Eq. (45) modifies to

$$\chi_m(Z, \lambda, R) \geq \left(\frac{1}{Z \times \lambda \times R} \right)^{\frac{1}{3}}. \quad (46)$$

In the future, this expression will provide us with the required path to determine the metallic character in confined systems. Now using the outcome in Eqs. (45) and (46), one can conjecture that if we have n number of parameters (a_i) in the Hamiltonian, then we get the relation as given below,

$$\chi_m(\prod a_i) \geq \chi_m^{th}(P) = \left(\frac{1}{\prod_{i=1}^n a_i} \right)^{\frac{1}{n}}. \quad (47)$$

Among these n parameters, if j of them become 1, then Eq. (47) can be expressed as

$$\chi_m(\prod a_i) \geq \chi_m^{th}(P) = \left(\frac{1}{\prod_{i=1}^{(n-j)} a_i} \right)^{\frac{1}{(n-j)}}. \quad (48)$$

The above relation provides a detailed illustration of the descriptor χ_m . Interestingly, all these derived relations converge to the conventional form, viz., Eq. (16), when $\chi_m^{th}(P)$ (when all a_i 's are unity) becomes unity.

(2) Sum (S): Adding Eqs. (37)–(40), one can express

$$(Z + \lambda + R_a + R_b)\chi_m(Z, \lambda, R_a, R_b) = K_1, \quad (49)$$

where

$$\begin{aligned} &\chi_m\left(1, \frac{\lambda}{Z}, ZR_a, ZR_b\right) + \chi_m\left(\frac{Z}{\lambda}, 1, \lambda R_a, \lambda R_b\right) \\ &+ \chi_m\left(ZR_a, \lambda R_a, 1, \left[\frac{R_b}{R_a}\right]\right) \\ &+ \chi_m\left(ZR_b, \lambda R_b, \left[\frac{R_a}{R_b}\right], 1\right) = K_1. \end{aligned} \quad (50)$$

Now we can write $K_1 \geq 4$, as all the components in Eq. (50) are ≥ 1 . Using this condition, one can rewrite Eq. (49) as

$$\begin{aligned} (Z + \lambda + R_a + R_b)\chi_m(Z, \lambda, R_a, R_b) &\geq 4, \\ \chi_m(Z, \lambda, R_a, R_b) &\geq \chi_m^{th}(S) \\ &= \frac{4}{(Z + \lambda + R_a + R_b)}. \end{aligned} \quad (51)$$

Thus, we have found another criterion for metallization in the form of $\chi_m^{th}(S)$. Further, when $R_a = 0$ and $R_b = R$, then Eq. (51) modifies to

$$\chi_m(Z, \lambda, R) \geq \frac{3}{(Z + \lambda + R)}. \quad (52)$$

Applying the expressions in Eqs. (51) and (52), one can deduce that for a Hamiltonian with n number of parameters (a_i), χ_m becomes

$$\chi_m(\prod a_i) \geq \chi_m^{th}(S) = \frac{n}{\sum_i a_i}. \quad (53)$$

This equation indicates that $\chi_m^{th}(S)$ depends on the nature of the parameters as well as on their numbers. Moreover, one may also derive a generalized expression of $\chi_m^{th}(S)$ in the following form:

$$\chi_m(\prod a_i) \geq \chi_m^{th}(S) = \left(\frac{n}{\sum_i a_i^b} \right)^{\frac{1}{nb}}, \quad (54)$$

where b is a real positive constant. Like $\chi_m^{th}(P)$, when all a_i 's are unity, all these relations nicely converge to Eq. (16).

From the foregoing discussion, we now present a comparative analysis of $\chi_m^{th}(P)$ and $\chi_m^{th}(S)$ in the following:

(1) The numerator in $\chi_m^{th}(P)$ is always 1. However, in $\chi_m^{th}(S)$, it is n . The numerator changes with a change in the count of the parameters. Moreover, the first quantity changes only with the environmental factors. On the contrary, the second quantity alters with the parameters and their numbers. It also depends on an arbitrary real constant b . This additional dependence may lead to an overestimation of $\chi_m^{th}(S)$.

(2) It is interesting to point out that when b is significantly large and any one of the a_i 's is greater than unity, then $\left(\frac{n}{\sum_i a_i^b}\right) \rightarrow 0$. But it is not permissible as a criterion of metallization. Therefore, a limiting value of b is required. This special situation is *not encountered* in the case of $\chi_m^{th}(P)$.

(3) In $\chi_m^{th}(S)$, if any one of the parameters becomes significantly small compared to the others, then its relative contribution appears negligible. But this situation is also *not observed* in $\chi_m^{th}(P)$.

The above three points thus suggest $\chi_m^{th}(P)$ to be relatively better than $\chi_m^{th}(S)$. From now onwards, throughout the manuscript, we use the *simplest forms* of $\chi_m^{th}(P)$ and $\chi_m^{th}(S)$ given in Eqs. (47) and (53), for illustrative purposes. These two conditions will now be used to discuss the metal-like character in *confined* and *shell-confined* (H-like ions, DP, EC-SCP) systems and ISP. Note that as $\chi_m^{th}(P)$, $\chi_m^{th}(S)$ are two different quantities, for a given set of parameters, they provide separate values. In this situation, we choose the lower χ_m^{th} as the threshold for metallization. Demonstrative results will be shown for the $1s, 2s, 2p, 3d$ states. Some other consequences of Eqs. (47) and (53) are discussed in the Appendix.

III. RESULT AND DISCUSSION

A. Metallization in CHA and SCHA

At the onset, it should be mentioned that in CHA, the analytical closed-form expression of $P_{n,\ell}$ is available [104,105,107–109]. Therefore, it is useful to begin the present demonstration by exploring $\zeta_{n,\ell}(=P_{n,\ell}V)$. Following [104,105,107–109], one can write

$$\begin{aligned} 3P_{n,\ell}V &= -R\left(\frac{d\mathcal{E}_{n,\ell}}{dR}\right) \\ &= \mathcal{E}_{n,\ell} + T_{n,\ell} = 2\mathcal{E}_{n,\ell} - C_{n,\ell} = 2T_{n,\ell} + C_{n,\ell}. \end{aligned} \quad (55)$$

Now, upon application of this relation, it modifies Eq. (20) as follows:

$$\begin{aligned} P_{n,\ell}\alpha_{n\ell}^{(1)} &= \zeta_{n,\ell} = \zeta_m \geq \frac{3}{4\pi}(\mathcal{E}_{n\ell} + T_{n,\ell}) = \frac{3}{4\pi}(2\mathcal{E}_{n\ell} - C_{n,\ell}) \\ &= \frac{3}{4\pi}(T_{n\ell} + C_{n,\ell}) = \zeta^{th}. \end{aligned} \quad (56)$$

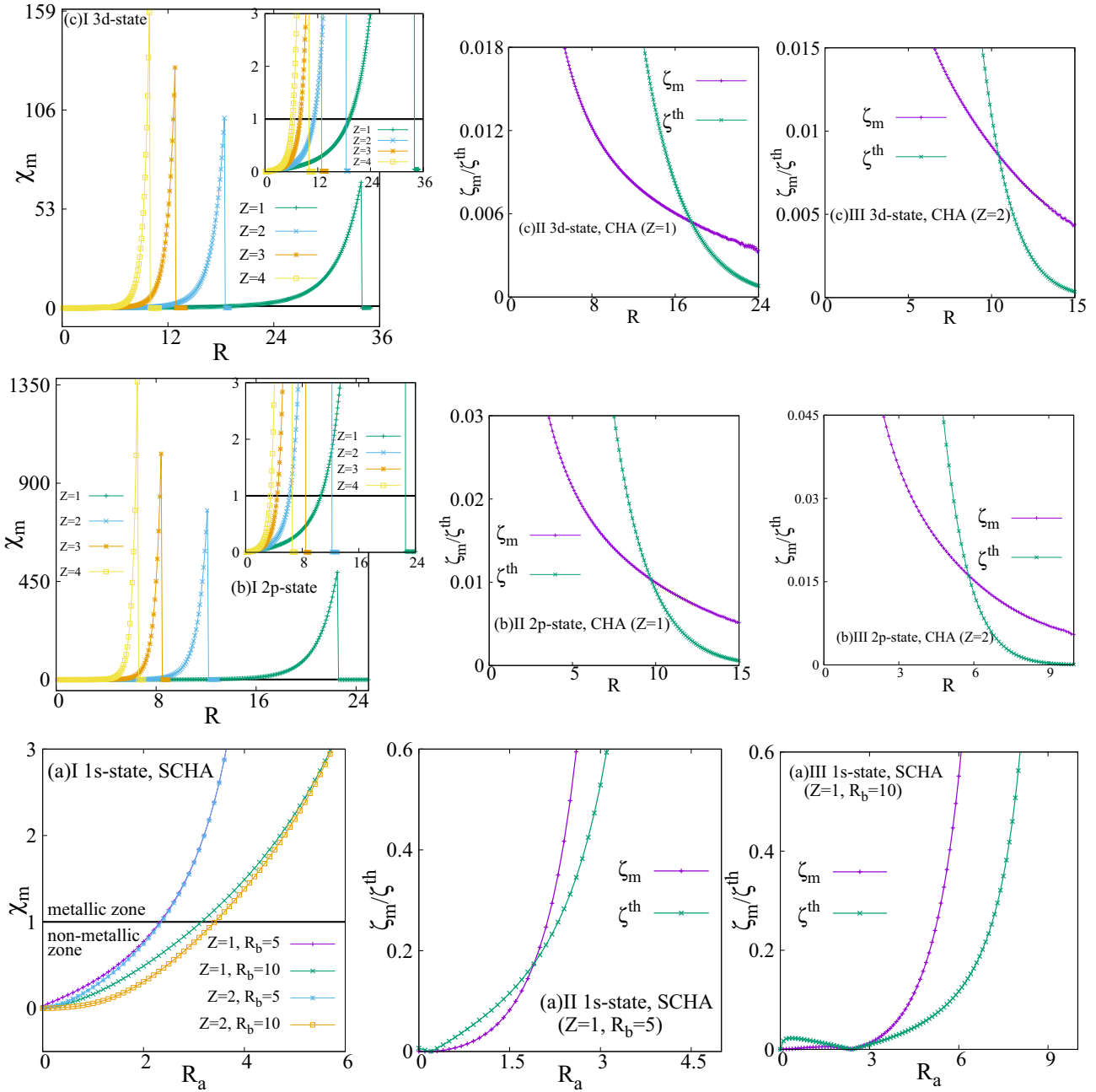


FIG. 2. Variation of (I) χ_m (in a.u.) and (II)–(III) ζ_m/ζ^{th} (in a.u.) for (a) $1s$, (b) $2p$, and (c) $3d$ states as a function of R_a [for the $1s$ state at $R_b = 5, 10$ (in a.u.)] or R (in a.u.) (for $2p, 3d$ states). See text for details.

Thus, according to Eq. (56), the metallic character can be observed when $\zeta_{n,\ell}(= \zeta_m)$ becomes larger than the ζ^{th} . Note that a similar such relation in SCHA is not known. In this endeavor, before going to probe the present condition, given by Eq. (47), it is important to review some of the conclusions of [83]. There, the major objective was to examine the existence of a metallic character in SCHA using HC. Two candid conclusions were reported: (i) in SCHA, the metallic character was predicted at the $\ell = 0$ states, and (ii) in CHA, no metallic pattern was observed. However, the calculation was restricted up to $R_b/R = 10$ in SCHA and CHA. In the present attempt, we have performed a thorough investigation by applying $\chi_m, \zeta_m, \zeta^{th}$ in the $1s, 2s, 3s, 4s, 2p, 3d$

states at $Z = 1, 2, 3, 4$. The calculated outcomes (metallization involving the $1s, 2p, 3d$ states) are plotted in Fig. 2. Here, the bottom (a) row represents the $1s$ state of SCHA ($R_b = 5, 10$). The middle (b) and top (c) rows represent the $2p, 3d$ states of CHA. Panels I illustrate the change of χ_m , while panels II and III demonstrate the alteration of ζ_m/ζ^{th} as a function of R_a/R . The figures in panels (b)I and (c)I are magnified in the inset plot to display the threshold of metallization. The following main conclusions can be drawn:

(1) χ_m, ζ_m both can explain the metallic pattern in CHA and SCHA. Also, ζ_m complements the results obtained by employing χ_m .

TABLE I. $\alpha_{n\ell}^{(1)}$, $\chi_m(n\ell)$ for $1s$, $2s$, $2p$, $3d$ states in CHA and SCHA. Metallic states are highlighted in bold font. See text for details.

CHA													
Z	λ	R_a	R_b	$\chi_m^{th}(P)$	$\chi_m^{th}(S)$	$\alpha_{1s}^{(1)}$	$\chi_m(1s)$	$\alpha_{2s}^{(1)}$	$\chi_m(2s)$	$\alpha_{2p}^{(1)}$	$\chi_m(2p)$	$\alpha_{3d}^{(1)}$	$\chi_m(3d)$
1	0	0	1	1	1	0.028792	0.028792	0.004414	0.004414	0.0171513	0.0171513	0.00894345	0.0089434
1	0	0	5	$\frac{1}{5}$	$\frac{1}{3}$	3.422454	0.027379	-21.106573	-0.168853	18.0892462	0.144714	7.21196971	0.0576957
1	0	0	8	$\frac{1}{8}$	$\frac{2}{9}$	4.453964	0.008699	-450.541668	-0.879964	203.884365	0.3982116	59.2654093	0.1157527
1	0	0	10	$\frac{1}{10}$	$\frac{2}{11}$	4.496814	0.004497	-2086.463707	-2.086464	793.323127	0.7933231	171.836687	0.171837
1	0	0	12	$\frac{1}{12}$	$\frac{2}{9}$	4.499828	0.002604	-8329.942227	-4.820568	2919.43908	1.6894902	431.846554	0.249911
2	0	0	5	$\sqrt{\frac{1}{10}}$	$\frac{2}{7}$	0.281051	0.002248	-130.403981	-1.043232	49.5826954	0.3966616	10.739793	0.085918
2	0	0	9	$\sqrt{\frac{1}{18}}$	$\frac{2}{11}$	0.281250	0.000386	7.0637078	0.0096896	10.748798	0.0147445	285.246944	0.391285
2	0	0	12	$\sqrt{\frac{1}{24}}$	$\frac{1}{7}$	0.281250	0.000163	7.4858069	0.0043320	10.993356	0.0063619	2632.57032	1.523502
SCHA													
Z	λ	R_a	R_b	$\chi_m^{th}(P)$	$\chi_m^{th}(S)$	$\alpha_{1s}^{(1)}$	$\chi_m(1s)$	$\alpha_{2s}^{(1)}$	$\chi_m(2s)$	$\alpha_{2p}^{(1)}$	$\chi_m(2p)$	$\alpha_{3d}^{(1)}$	$\chi_m(3d)$
1	0	1.5	2	$\sqrt{\frac{1}{3}}$	$\frac{2}{3}$	6.201980	1.340968	6.144904	1.328628	0.000824	0.0001782	0.0008244	0.000178
1	0	3	8	$\sqrt{\frac{1}{24}}$	$\frac{1}{4}$	527.1729790	1.086955	512.997468	1.057727	8.314061	0.0171424	8.4883946	0.017502
1	0	1	12	$\frac{1}{12}$	$\frac{3}{14}$	191.1721328	0.1106961	501.362811	0.290309	147.5111	0.0854147	277.05547	0.1604259
1	0	1	15	$\frac{1}{15}$	$\frac{3}{17}$	204.610181	0.0606432	1088.76830	0.322694	241.63929	0.071618	823.36412	0.244032
2	0	2	5	$(\frac{1}{20})^{\frac{1}{3}}$	$\frac{1}{3}$	87.0959196	0.7444096	86.1225205	0.736090	1.0711982	0.0091555	1.091477	0.0093289
2	0	3	8	$(\frac{1}{48})^{\frac{1}{3}}$	$\frac{1}{3}$	488.5711833	1.0073633	523.019593	1.078391	8.0246547	0.0165555	8.3249448	0.0171648
2	0	0.1	12	$(\frac{5}{12})^{\frac{1}{3}}$	$\frac{10}{47}$	1.2280053	0.0007107	-9.119076	-0.005277	24.8620099	0.0143555	2135.8451	1.236022
2	0	0.5	12	$(\frac{1}{12})^{\frac{1}{3}}$	$\frac{6}{29}$	12.9305981	0.0074835	217.2985067	0.125760	19.4197955	0.0112391	333.45412	0.192985

(2) CHA:

(a) In s -wave states, $\chi_m < 1$ (always); further, $\zeta_m > \zeta^{th}$ (never).

(b) In $2p$, $3d$ states, the metallic character can be seen. Both χ_m and ζ^m support the existence of such pattern for the $\ell \neq 0$ states.

(c) In $2p$ and $3d$ states, the metallic region decreases with an increase in Z . Additionally, the intersection point between ζ_m and ζ^{th} gets left shifted with Z .

(d) In $2p$ and $3d$ states, at a certain Z value, χ_m increases with R to reach a maximum value and finally falls down below 1.

(3) SCHA:

(a) A metallic signature is observed in s -wave states. At a given (R_b, Z) , χ_m increases with a rise in R_a . There exists a threshold R_a after which $\chi_m > 1$. Similarly, at a given (R_b, Z) , both ζ_m and ζ^{th} decrease with R_a . However, at a characteristic R_a , ζ_m becomes greater than ζ^{th} .

(b) For the $2p$ state, χ_m is always less than 1, and ζ_m never exceeds ζ^{th} .

(c) For the $3d$ state ($Z = 1, 2$) at a fixed R_b , $\chi_m > 1$ at some small value of R_a . On the contrary, with a rise in R_a , it becomes less than 1. However, for the $Z > 2$ cases, such phenomena of metallization are not seen.

Now the focus is to examine the conditions derived in Eqs. (47) and (53). For CHA and SCHA, this extended form is modified to $\chi_m \geq \frac{1}{\sqrt{Z \times R}}$, $\chi_m \geq (\frac{2}{Z+R})$ and $\chi_m \geq \frac{1}{(Z \times R_a \times R_b)^{\frac{1}{3}}}$, $\chi_m \geq (\frac{3}{Z+R_a+R_b})$. In CHA, $\chi_m^{th}(P) = \frac{1}{\sqrt{Z \times R}} > 1$ if $R < \frac{1}{Z}$. Similarly, in SCHA, $\chi_m^{th}(P) = \frac{1}{(Z \times R_a \times R_b)^{\frac{1}{3}}} > 1$,

when $R_a R_b < \frac{1}{Z}$. Table I delineates the numerical results of $\chi_m^{th}(P)$, $\chi_m^{th}(S)$, χ_m , $\alpha_{n,\ell}^{(1)}$ in $1s$, $2s$, $2p$, $3d$ states for CHA and SCHA in the upper and lower sections. These are tabulated for eight selected separate sets of Z , R_a , R_b (different for CHA and SCHA). In some cases, the $\chi_m^{th}(P)$ value is greater than $\chi_m^{th}(S)$, and vice versa. In metallic cases, χ_m is greater than both thresholds. Similarly, in nonmetallic cases, it is less than either of these quantities. Metallic patterns are marked with bold font. A detailed analysis elicits several conclusions and they are as follows:

(1) CHA:

(a) For $1s$, $2s$ states, $\chi_m < \chi_m^{th}$ (always). Therefore, the metallic character is not seen.

(b) For $2p$, $3d$ states, the metallic characteristic is observed. In the $2p$ state, $\chi_m > \chi_m^{th}$ at $R \approx 8$ for $Z = 1$ and $R \approx 5$ for $Z = 2$. Further, in the $3d$ states, χ_m overcomes χ_m^{th} at $R \approx 10, 9$ for $Z = 1, 2$, respectively. Thus, employing the

TABLE II. $\alpha_{n\ell}^{(1)}$, $\chi_m(n\ell)$ values for $1s, 2s, 2p, 3d$ states in CDP and SCDP. Metallic states are highlighted in bold font. See text for details.

CDP													
Z	λ_1	R_a	R_b	$\chi_m^{th}(P)$	$\chi_m^{th}(S)$	$\alpha_{1s}^{(1)}$	$\chi_m(1s)$	$\alpha_{2s}^{(1)}$	$\chi_m(2s)$	$\alpha_{2p}^{(1)}$	$\chi_m(2p)$	$\alpha_{3d}^{(1)}$	$\chi_m(3d)$
1	3	0	5	$\sqrt{\frac{1}{15}}$	$\frac{1}{3}$	19.109231	0.152874	1.471052	0.011768	11.335210	0.0906817	5.3753898	0.0430031
1	3	0	10	$\sqrt{\frac{1}{30}}$	$\frac{3}{14}$	327.30979	0.32731	42.08979	0.042098	172.381668	0.1723817	84.8148705	0.0848149
1	0.7	0	15	$\sqrt{\frac{2}{21}}$	$\frac{30}{167}$	28.447601	0.00843	6070.83704	1.798766	-818.245723	-0.242443	500.162473	0.1481963
1	0.6	0	20	$\sqrt{\frac{1}{12}}$	$\frac{5}{36}$	16.928366	0.002116	10968.4142	1.371052	181.315540	0.022664	1588.579581	0.1985724
1	3	0	20	$\sqrt{\frac{1}{60}}$	$\frac{1}{8}$	5498.63355	0.68733	975.261462	0.121907	2631.30019	0.328913	1352.59487	0.169074
1	4	0	10	$\sqrt{\frac{1}{40}}$	$\frac{1}{5}$	344.261325	0.34426	62.28041	0.062280	164.036308	0.164036	84.601556	0.084601
1	5	0	15	$\sqrt{\frac{1}{75}}$	$\frac{1}{7}$	1799.15502	0.53308	383.92066	0.113754	803.431212	0.238054	427.800342	0.126756
2	4	0	15	$(\frac{1}{120})^{\frac{1}{3}}$	$\frac{1}{7}$	1637.78292	0.48527	175.79271	0.052087	885.676827	0.262423	428.098198	0.126844
SCDP													
Z	λ_1	R_a	R_b	$\chi_m^{th}(P)$	$\chi_m^{th}(S)$	$\alpha_{1s}^{(1)}$	$\chi_m(1s)$	$\alpha_{2s}^{(1)}$	$\chi_m(2s)$	$\alpha_{2p}^{(1)}$	$\chi_m(2p)$	$\alpha_{3d}^{(1)}$	$\chi_m(3d)$
1	0.005	3	5	$(\frac{40}{27})^{\frac{1}{3}}$	$\frac{800}{1801}$	165.909136	1.692950	161.858188	1.651614	0.211711	0.002160	0.212007	0.002163
1	0.005	5	10	$4^{\frac{1}{3}}$	$\frac{800}{3201}$	1969.388635	2.250729	1925.745173	2.200851	8.272785	0.009454	8.321984	0.009511
1	1	1.2	2	$\sqrt{\frac{5}{12}}$	$\frac{10}{13}$	4.262406	0.679593	4.139491	0.659995	0.005424	0.000865	0.005431	0.000866
1	2	2	5	$(\frac{1}{20})^{\frac{1}{3}}$	$\frac{2}{5}$	84.642595	0.723441	93.685705	0.800732	1.0902882	0.009319	1.096345	0.00937
2	1	1	15	$\frac{1}{15}$	$\frac{4}{19}$	1886.33083	0.559078	712.167126	0.211075	637.13395	0.188837	434.612171	0.128812
1	6	1	12	$\sqrt{\frac{1}{72}}$	$\frac{1}{5}$	1017.16582	0.58898	500.704442	0.289927	221.729741	0.128391	167.059065	0.096733
2	5	1	10	$(\frac{1}{100})^{\frac{1}{3}}$	$\frac{2}{9}$	522.112782	0.522635	278.578518	0.278857	98.425239	0.098524	78.177816	0.078257
2	1	1	20	$\sqrt{\frac{1}{40}}$	$\frac{1}{6}$	6862.778876	0.857955	1697.30985	0.212190	2398.740394	0.299879	1411.938337	0.176514
3	4	2	15	$(\frac{1}{360})^{\frac{1}{4}}$	$\frac{1}{6}$	2996.594701	0.889989	1819.141066	0.540285	420.065662	0.12476	363.565429	0.107979
4	0.5	2	10	$(\frac{1}{40})^{\frac{1}{4}}$	$\frac{8}{33}$	427.576435	0.431025	575.104856	0.579743	56.179984	0.056633	70.135258	0.070701

present condition, the metallic nature can be expected at lower R or higher $P_{n,\ell}$.

(2) SCHA:

(a) The metallic pattern is obeyed in $1s, 2s$ states. At a fixed R_b , the threshold value of R_a (for metallization) decreases. For example, in the $1s$ state ($Z = 1$) at $R_b = 5, 10$, the threshold values of R_a are approximately 1.3, 1.4, respectively. However, applying HC, the previous cutoff values were 2.3295, 3.1477 successively [83].

(b) Interestingly, χ_m becomes greater than χ_m^{th} for both the $2p$ and $3d$ states.

(3) The proposed criterion complements the observation obtained by employing HC and ζ_m . Further, it also explains the metallic pattern in the $2p$ state of SCHA.

B. Metallization in confined and shell-confined DP and ECSCP

In the Herzfeld framework, the metal-like behavior of confined and shell-confined DP (CDP and SCDP) is yet to

be explored. In this section, at first we apply the conventional HC ($\chi_m \geq 1$) to examine the metallic pattern in CDP and SCDP. Then, we shall discuss the modified criterion ($\chi_m \geq \chi_m^{th}$) on them. Table II displays the numerical values of $\alpha_{n\ell}^{(1)}$, χ_m , $\chi_m^{th}(P)$, $\chi_m^{th}(S)$ for $1s, 2s, 2p, 3d$ states involving CDP and SCDP. A careful analysis indicates that in CDP, the metallic feature can be observed only in the $2s$ state, as per the original HC. However, in SCDP, it can be expected in both the $1s$ and $2s$ states. Thus, by applying the modified conditions available in Eq. (57), one may expect a metal-like pattern in all of these four states ($1s, 2s, 2p, 3d$) of CDP.

Now let us discuss χ_m^{th} . For CDP and SCDP, Eqs. (47) and (53) read as

$$\chi_m \geq \frac{1}{(Z \times \lambda_1 \times R)^{\frac{1}{3}}} = \chi_m^{th}(P) \text{ and } \chi_m \geq \left(\frac{3}{Z + \lambda_1 + R} \right) = \chi_m^{th}(S) \text{ (CDP),}$$

$$\begin{aligned} \chi_m &\geq \frac{1}{(Z \times \lambda_1 \times R_a \times R_b)^{\frac{1}{4}}} \\ &= \chi_m^{th}(P) \text{ and } \chi_m \geq \left(\frac{4}{Z + \lambda_1 + R_a + R_b} \right) \\ &= \chi_m^{th}(S) \text{ (SCDP)}. \end{aligned} \tag{57}$$

It should be kept in mind that in CDP, when $R < \frac{1}{\lambda \times Z}$, then $\chi_m^{th}(P) > 1$. Similarly, in SCDP, if $R_a R_b < \frac{1}{\lambda \times Z}$, then again $\chi_m > 1$. An examination of Table II implies that the metallic character can be observed in $1s, 2s, 2p, 3d$ of both CDP and SCDP.

Now we move to pursue confined ECSCP (CECSCP) and shell-confined ECSCP (SCECSCP). Similar to DP, the metal-like behavior in these two systems has not been investigated

yet. Equations (47) and (53) in this case read as

$$\begin{aligned} \chi_m &\geq \frac{1}{(Z \times \lambda_2 \times R)^{\frac{1}{3}}} \\ &= \chi_m^{th}(P) \text{ and } \chi_m \geq \left(\frac{3}{Z + \lambda_2 + R} \right) = \chi_m^{th}(S), \\ \chi_m &\geq \frac{1}{(Z \times \lambda_2 \times R_a \times R_b)^{\frac{1}{4}}} \\ &= \chi_m^{th}(P) \text{ and } \chi_m \geq \left(\frac{4}{Z + \lambda_2 + R_a + R_b} \right) = \chi_m^{th}(S). \end{aligned} \tag{58}$$

Now Table III delineates the numerical outcomes in CECSCP and SCECSCP for the same set of parameters at the same set of $Z, \lambda_2, R_a, R, R_b$ mentioned in Table II connecting the

TABLE III. $\alpha_{n\ell}^{(1)}, \chi_m(n\ell)$ values for $1s, 2s, 2p, 3d$ states in *confined* and *shell-confined* ECSCP. Metallic states are highlighted in bold font. See text for details.

CECSCP													
Z	λ_2	R_a	R_b	$\chi_m^{th}(P)$	$\chi_m^{th}(S)$	$\alpha_{1s}^{(1)}$	$\chi_m(1s)$	$\alpha_{2s}^{(1)}$	$\chi_m(2s)$	$\alpha_{2p}^{(1)}$	$\chi_m(2p)$	$\alpha_{3d}^{(1)}$	$\chi_m(3d)$
1	3	0	5	$\sqrt{\frac{1}{15}}$	$\frac{1}{3}$	22.35614	0.178849	4.61301	0.03690	9.92192	0.07937	5.24135	0.04193
1	3	0	10	$\sqrt{\frac{1}{30}}$	$\frac{3}{14}$	361.60966	0.3616	82.99628	0.082996	155.88079	0.15588	84.39217	0.08439
1	0.7	0	15	$\sqrt{\frac{2}{21}}$	$\frac{30}{167}$	350.70554	0.10391	-20460.73597	-6.06244	8082.38001	2.39478	407.19846	0.12065
1	0.6	0	20	$\sqrt{\frac{1}{12}}$	$\frac{5}{36}$	83.63644	0.01045	14974.59512	1.87182	-730.13219	-0.09127	1284.26877	0.16053
1	3	0	20	$\sqrt{\frac{1}{60}}$	$\frac{1}{8}$	5802.27299	0.72528	1359.48149	0.16993	2484.04397	0.31051	1351.62413	0.16895
1	4	0	10	$\sqrt{\frac{1}{40}}$	$\frac{1}{5}$	362.72302	0.36272	84.93378	0.08493	155.24372	0.15524	84.45772	0.08446
1	5	0	15	$\sqrt{\frac{1}{75}}$	$\frac{1}{7}$	1838.71230	0.54480	434.12775	0.12863	784.54805	0.23246	427.70510	0.12673
2	4	0	15	$(\frac{1}{120})^{\frac{1}{3}}$	$\frac{1}{7}$	1829.92476	0.5422	422.21408	0.12510	788.85887	0.23374	427.63232	0.12671
SCECSCP													
Z	λ_2	R_a	R_b	$\chi_m^{th}(P)$	$\chi_m^{th}(S)$	$\alpha_{1s}^{(1)}$	$\chi_m(1s)$	$\alpha_{2s}^{(1)}$	$\chi_m(2s)$	$\alpha_{2p}^{(1)}$	$\chi_m(2p)$	$\alpha_{3d}^{(1)}$	$\chi_m(3d)$
1	0.005	3	5	$(\frac{40}{27})^{\frac{1}{3}}$	$\frac{800}{1801}$	165.909136	1.69295	161.85819	1.65161	0.21171	0.00216	0.21201	0.00216
1	0.005	5	10	$4^{\frac{1}{3}}$	$\frac{800}{3201}$	1969.35464	2.25069	1925.7546	2.20086	8.27270	0.00955	8.32192	0.00951
1	1	1.2	2	$\sqrt{\frac{5}{12}}$	$\frac{10}{13}$	4.26402	0.67985	4.13903	0.65992	0.00543	0.00086	0.00543	0.00087
1	2	2	5	$(\frac{1}{20})^{\frac{1}{3}}$	$\frac{2}{5}$	93.70837	0.80093	84.65575	0.72355	1.08986	0.00932	1.09589	0.00937
2	1	1	15	$\sqrt{\frac{1}{15}}$	$\frac{4}{19}$	2516.52307	0.74586	1209.96756	0.35862	540.52441	0.16020	400.40297	0.11867
1	6	1	12	$\sqrt{\frac{1}{72}}$	$\frac{1}{5}$	1017.17687	0.58899	500.74971	0.28995	221.72672	0.12839	167.05824	0.09673
2	5	1	10	$(\frac{1}{100})^{\frac{1}{3}}$	$\frac{2}{9}$	522.15	0.52267	278.61561	0.27889	98.4169	0.098515	78.17432	0.07825
2	1	1	20	$\sqrt{\frac{1}{40}}$	$\frac{1}{6}$	7352.37264	0.91916	3225.75953	0.40327	1873.40216	0.23421	1311.00250	0.1639
3	4	2	15	$(\frac{1}{360})^{\frac{1}{4}}$	$\frac{1}{6}$	2996.61654	0.88999	1819.16476	0.54029	420.0616	0.12476	363.56326	0.10798
4	0.5	2	10	$(\frac{1}{40})^{\frac{1}{4}}$	$\frac{8}{33}$	843.45417	0.85026	487.43521	0.49137	64.21420	0.06473	57.21745	0.05768

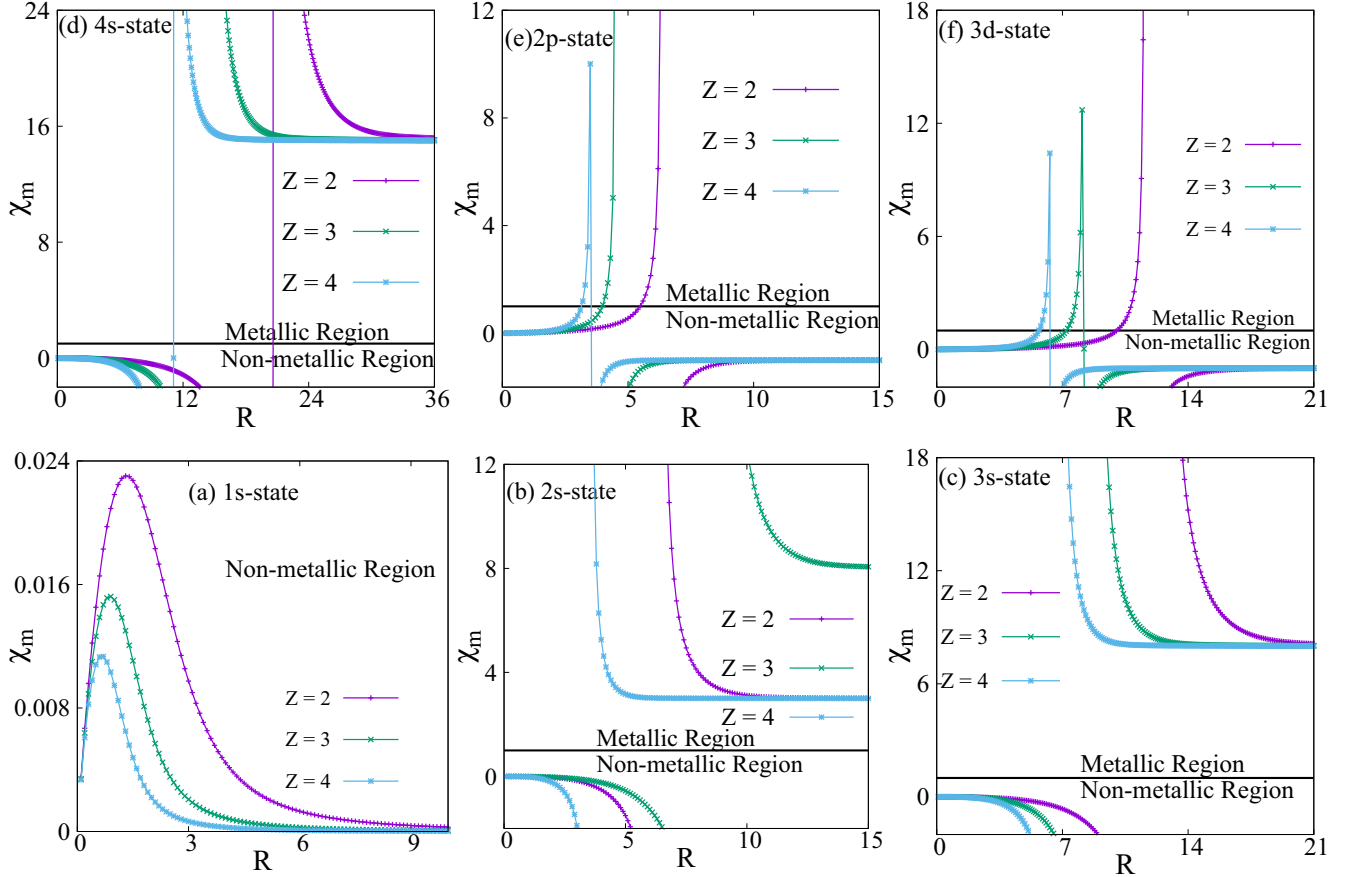


FIG. 3. Variation of χ_m (in a.u.) for (a) $1s$, (b) $2s$, (c) $3s$, (d) $4s$, (e) $2p$, and (f) $3d$ states as a function of R (in a.u.) at $Z = 2, 3, 4$. See text for details.

$1s, 2s, 2p, 3d$ states. It reveals an analogous conclusion to DP. Note that HC can only explain the metallic feature in the $2s$ state of CECS and $1s, 2s$ of SCECS. However, Eq. (58) shows the metallicity in the $1s, 2s, 2p, 3d$ states under both kinds of confinement.

C. Metallization in ISP

Now the focus is on ISP, where, like the other two plasmas, the metallic property has not yet been probed. Like the previous two sections, we first apply HC in ISP, and then extend the discussion to Eq. (47). Before going into the detailed analysis, it should be kept in mind that for ISP, $Z \geq 2$. Figure 3 displays the plots of χ_m as a function of R in the $1s, 2s, 3s, 4s, 2p, 3d$ states involving three Z , namely, 2,3,4. Figure 3(a) indicates that χ_m for the $1s$ state is always less than 1. Therefore, the metallic behavior is not recorded. However, Figs. 3(b)–3(f) portray that at a certain range of R , χ_m in the $2s, 3s, 4s, 2p, 3d$ states becomes larger than 1. However, for a given state, this metallic region changes with Z . Analysis of Figs. 3(b)–3(d) suggests that for $2s, 3s, 4s$ states, with an increase in R , χ_m decreases (becomes negative) and then suddenly rises abruptly to indicate a metallic property. But an opposite pattern is noticed in the $2p, 3d$ states in Figs. 3(e) and 3(f). It increases with a rise in R to show the metallic feature, and then reaches a maximum value and suddenly jumps down to lower than

unity. In essence, the metallic pattern can be seen in all five of these excited states, but the ground state is nonmetallic.

The usual scaling transformation with respect to λ of Eq. (6) says that in ISP, $\lambda = (\frac{1}{2R^3})^{\frac{1}{4}}$. In that case, Eqs. (47) and (53) can be projected as

$$\begin{aligned} \chi_m &\geq \chi_m^{th}(P) \\ &= \left(\frac{2^{\frac{1}{4}}}{Z^{\frac{1}{3}} \times R^{\frac{1}{12}}} \right) \text{ and } \chi_m \geq \chi_m^{th}(S) = \left(\frac{3}{Z + R + \lambda} \right). \end{aligned} \quad (59)$$

Table IV illustrates the calculated values $\chi_m, \chi_m^{th}(P), \chi_m^{th}(S), \alpha_{nl}^{(1)}$ at 12 sets of Z, λ and R in the $1s, 2s, 2p, 3d$ states. These outcomes complement the observation found by applying HC. The metallic feature is not reported in the $1s$ state; however, in other states ($2s, 2p, 3d$), this characteristic can be found.

D. Hydrogenlike ions and plasmas inside fullerene cavity

Finally, we arrive at a situation where the H-like ions, DP, and ECSCP are trapped inside a fullerene cavity. As usual, we have applied the HC in the $1s, 2s$ states. One cannot derive Eq. (47) for these systems using the scaling concept. A thorough investigation is necessary. In the future, we shall pursue in this direction. However, we conjecture an empirical

TABLE IV. $\alpha_{n\ell}^{(1)}$, $\chi_m(n\ell)$ for the $1s$, $2s$, $2p$, $3d$ states in ISP. Metallic states are highlighted in bold font. See text for details.

ISP												
Z	$(\frac{1}{2R^3})^{\frac{1}{4}}$	R	$\chi_m^{th}(P)$	$\chi_m^{th}(S)$	$\alpha_{1s}^{(1)}$	$\chi_m(1s)$	$\alpha_{2s}^{(1)}$	$\chi_m(2s)$	$\alpha_{2p}^{(1)}$	$\chi_m(2p)$	$\alpha_{3d}^{(1)}$	$\chi_m(3d)$
2	0.23414	5.5	0.72953	0.38789	0.28388	0.00171	-489.42904	-2.94172	171.23976	1.02924	17.63837	0.10602
2	0.21935	6	0.72426	0.36499	0.28330	0.00131	-1776.12141	-8.22278	601.64237	2.78538	27.88738	0.12911
2	0.20657	6.5	0.71945	0.34457	0.28287	0.00103	9684.22515	35.26345	-3217.14850	-11.7147	43.30084	0.15767
2	0.17678	8	0.70711	0.29479	0.28211	0.00055	2049.7721	4.00346	-669.86708	-1.30833	154.0665	0.30091
2	0.14954	10	0.69408	0.24692	0.28169	0.00028	3121.76752	3.12177	-1026.53077	-1.02653	979.04436	0.97904
2	0.13922	11	0.68859	0.22832	0.28158	0.00020	4064.78465	3.05393	-1340.92491	-1.00746	4071.5293	3.0590
3	0.29730	4	0.65445	0.41111	0.05582	0.00087	-15.06549	-0.235398	67.54544	1.0554	5.45227	0.08519
3	0.17678	8	0.61771	0.26841	0.05559	0.00011	-5319.65601	-10.38995	-513.37676	-1.00269	3173.7898	6.19881
3	0.16183	9	0.61168	0.24667	0.05558	0.00008	34963.03344	47.96027	-729.23835	-1.00033	-1551.23814	-2.1279
4	0.36889	3	0.60903	0.40712	0.01764	0.00065	-50.94067	-1.88669	17.55851	0.65031	1.71588	0.06355
4	0.29730	4	0.59460	0.34906	0.01760	0.00027	336.56034	5.25876	-111.38035	-1.74032	9.01553	0.14087
4	0.21935	6	0.57485	0.28369	0.01759	0.00008	652.78524	3.02215	-216.73912	-1.00342	444.19117	2.05644

relation, based on the observations we have obtained so far. With a rise in Z , the effective volume decreases. However, the effective volume increases with a rise in V_1 , Δ , γ , and R_0 . Therefore, one can obtain

$$\chi_m \geq \chi_m^{th}(P) = \left(\frac{1}{Z \times \lambda \times V_1 \times \Delta \times \gamma \times R_0 \times R} \right)^{\frac{1}{7}},$$

$$\chi_m \geq \chi_m^{th}(S) = \left(\frac{7}{Z + \lambda + V_1 + \Delta + \gamma + R_0 + R} \right). \quad (60)$$

For H-like systems, it becomes

$$\chi_m \geq \chi_m^{th}(P) = \left(\frac{1}{Z \times V_1 \times \Delta \times \gamma \times R_0 \times R} \right)^{\frac{1}{6}},$$

$$\chi_m \geq \chi_m^{th}(S) = \left(\frac{6}{Z + V_1 + \Delta + \gamma + R_0 + R} \right). \quad (61)$$

Sample results are presented in Table V at different sets of the Z , λ , R value keeping V_1 , Δ , γ , R_0 fixed at experimental values of 0.302, 5.8, 1.89, 0.1 a.u., respectively. According

to HC, the $2s$ state of DP, ECSCP, and H-like ions becomes metallic under high pressure. But, the $1s$ state always remains nonmetallic. On the contrary, using Eq. (61), one can observe metallic behavior in the $1s$ state of ECSCP. Unfortunately, similar results are not observed in DP and H-like ions. However, for the $2s$ state, Eqs. (60) and (61) complement the results obtained by employing HC. For a more elaborate picture, more works are necessary.

IV. CONCLUSION

Metallization conditions [$\chi_m(\prod a_i) \geq (\frac{1}{\prod_{i=1}^n a_i})^{\frac{1}{n}}$, $\chi_m(\prod a_i) \geq \frac{n}{\sum_{i=1}^n a_i}$] have been proposed for confined monatomic systems under pressure by invoking the HC and scaling concept. The present form incorporates the effect of the environment by including Z , λ and the boundary condition, etc. One can use this to explain metallicity in $\ell \geq 0$ states. In these conditions, the threshold value of metallization remains unchanged. However, a new volume correction term is introduced. The volume of a system varies with variation of charge, screen-

TABLE V. $\alpha_{n\ell}^{(1)}$, $\chi_m(n\ell)$, χ_m^{th} for the $1s$, $2s$ states in the H atom, DP, and ECSCP encapsulated inside a fullerene cavity (experimental values of V_1 , Δ , γ , R_0 are used). Metallic states are highlighted in bold font. See text for details.

H-like ion in fullerene								
Z	λ	R	$\chi_m^{th}(P)$	$\chi_m^{th}(S)$	$\alpha_{1s}^{(1)}$	$\chi_m(1s)$	$\alpha_{2s}^{(1)}$	$\chi_m(2s)$
1	0	8.0	0.82301	0.35104	4.74411	0.00927	2455.46032	4.79582
2	0	8.5	0.74979	0.32272	0.28125	0.00046	1075.46513	1.75122
DP in fullerene								
Z	λ_1	R	$\chi_m^{th}(P)$	$\chi_m^{th}(S)$	$\alpha_{1s}^{(1)}$	$\chi_m(1s)$	$\alpha_{2s}^{(1)}$	$\chi_m(2s)$
1	1	8.5	0.81309	0.37651	325.73794	0.53041	-110.54169	-0.179998
2	1	9.0	0.74269	0.36665	0.69985	0.00096	851.85352	1.16852
ECSCP in fullerene								
Z	λ_2	R	$\chi_m^{th}(P)$	$\chi_m^{th}(S)$	$\alpha_{1s}^{(1)}$	$\chi_m(1s)$	$\alpha_{2s}^{(1)}$	$\chi_m(2s)$
1	1	10.0	0.78708	0.36665	942.00971	0.94201	39.742268	0.039742
2	1	9.0	0.74269	0.36665	1.216007	0.00167	915.65709	1.25604

ing constant, and boundary. Moreover, the transfer of phase also alters the volume. Therefore, in the present work, an environmental correction is done on volume. Thus we propose $[(\prod_{i=1}^n a_i)^{\frac{1}{n}} \frac{\alpha_{nl}^{(1)}}{V} \geq 1, (\sum_{i=1}^n a_i) \frac{\alpha_{nl}^{(1)}}{V} \geq n]$ as two effective expressions of metallization in the framework of Herzfeld. Besides this, a different descriptor in the form of χ_m has been proposed to determine the metal-like properties in systems under high pressure. Apart from that, we have recast the conventional HC in terms of state pressure. A criterion has been designed based on that result. In the future, the derivation of $(\frac{d\mathcal{E}_{nl}}{dR})$ for a given confined system will provide us with the concrete analytical expression of ζ_m^{th} .

The applicability of this scheme has been tested and verified by doing pilot calculations on a total of eight different confined and shell-confined systems. It reveals that the metallic character can be observed in systems trapped under multimegabar pressure. It is worth mentioning that these relations can be applied to other atomic and ionic systems under such stressed condition. There are several open questions which may lead to an important conclusion and require further scrutiny, such as the use of these HC in determining metallic characteristics in atomic and molecular clusters and solids under high pressure.

ACKNOWLEDGMENTS

Financial support from BRNS, India (Grant No. 58/14/03/2019-BRNS/10255) is gratefully acknowledged. Partial financial assistance from SERB, India (Grant No. CRG/2019/000293) is appreciated. Critical constructive comments from two anonymous referees are greatly appreciated.

APPENDIX: ADDITIONAL DISCUSSION ON METALLIZATION

Here, we enumerate several auxiliary forms of Eqs. (45), (46), (51), and (52). At first, from Eqs. (45) and (51), the following situations may be conceived:

(1) When $Z = \lambda = R_b = 1$, $\chi_m(P)(1, 1, R_a, 1) \geq \frac{1}{R_a}$, and $\chi_m(S)(1, 1, R_a, 1) \geq (\frac{4}{R_a+3})$, $R_a < 1$.

(2) When $Z = \lambda = R_a = 1$, $\chi_m(P)(1, 1, 1, R_b) \geq \frac{1}{R_b}$, and $\chi_m(S)(1, 1, R_b, 1) \geq (\frac{4}{R_b+3})$, $R_b > 1$.

(3) When $Z = \lambda = 1$, $\chi_m(P)(1, 1, R_a, R_b) \geq \frac{1}{\sqrt{R_a \times R_b}}$, and $\chi_m(S)(1, 1, R_a, R_b) \geq (\frac{4}{R_a+R_b+2})$.

(4) When $\lambda = R_a = 1$, $\chi_m(P)(Z, 1, 1, R_b) \geq \frac{1}{\sqrt{Z \times R_b}}$, and $\chi_m(S)(Z, 1, 1, R_b) \geq (\frac{4}{Z+R_b+2})$, $R_b > 1$.

(5) When $Z = R_a = 1$, $\chi_m(P)(1, \lambda, 1, R_b) \geq \frac{1}{\sqrt{\lambda \times R_b}}$, and $\chi_m(S)(S)(1, \lambda, 1, R_b) \geq (\frac{4}{\lambda+R_b+2})$, $R_b > 1$.

(6) When $\lambda = R_b = 1$, $\chi_m(P)(Z, 1, R_a, 1) \geq \frac{1}{\sqrt{Z \times R_a}}$, and $\chi_m(S)(S)(Z, 1, R_a, 1) \geq (\frac{4}{Z+R_a+2})$, $R_a < 1$.

(7) When $Z = R_a = 1$, $\chi_m(P)(1, \lambda, 1, R_b) \geq \frac{1}{\sqrt{\lambda \times R_b}}$, and $\chi_m(S)(1, \lambda, 1, R_b) \geq (\frac{4}{\lambda+R_b+2})$, $R_b > 1$.

(8) When $Z = 1$, $\chi_m(P)(1, \lambda, R_a, R_b) \geq \frac{1}{(\lambda \times R_a \times R_b)^{\frac{1}{3}}}$, and $\chi_m(S)(1, \lambda, R_a, R_b) \geq (\frac{4}{\lambda+R_a+R_b+1})$.

(9) When $\lambda = 1$, $\chi_m(P)(Z, 1, R_a, R_b) \geq \frac{1}{(Z \times R_a \times R_b)^{\frac{1}{3}}}$, and $\chi_m(S)(Z, 1, R_a, R_b) \geq (\frac{4}{Z+R_a+R_b+1})$.

(10) When $R_a = 1$, $\chi_m(P)(Z, \lambda, 1, R_b) \geq \frac{1}{(Z \times \lambda \times R_b)^{\frac{1}{3}}}$, and $\chi_m(S)(Z, \lambda, 1, R_b) \geq (\frac{4}{Z+\lambda+R_b+1})$, $R_b > 1$.

(11) When $R_b = 1$, $\chi_m(P)(Z, \lambda, R_a, 1) \geq \frac{1}{(Z \times \lambda \times R_a)^{\frac{1}{3}}}$, and $\chi_m(S)(Z, \lambda, R_a, 1) \geq (\frac{4}{Z+\lambda+R_a+1})$, $R_a < 1$.

Likewise, a consideration of Eqs. (46) and (52) leads to the following:

(1) When $Z = \lambda = 1$, $\chi_m(P)(1, 1, R) \geq \frac{1}{R}$ and $\chi_m(S)(1, 1, R) \geq (\frac{3}{R+2})$.

(2) When $Z = R = 1$, $\chi_m(P)(1, \lambda, 1) \geq \frac{1}{\lambda}$ and $\chi_m(S)(1, \lambda, 1) \geq (\frac{3}{\lambda+2})$.

(3) When $\lambda = R = 1$, $\chi_m(P)(Z, 1, 1) \geq \frac{1}{Z}$ and $\chi_m(S)(Z, 1, 1) \geq (\frac{3}{Z+2})$.

(4) When $R = 1$, $\chi_m(P)(Z, \lambda, 1) \geq \frac{1}{\sqrt{Z \times \lambda}}$ and $\chi_m(S)(Z, \lambda, 1) \geq (\frac{3}{Z+\lambda+1})$.

(5) When $Z = 1$, $\chi_m(P)(1, \lambda, R) \geq \frac{1}{\sqrt{\lambda \times R}}$ and $\chi_m(S)(1, \lambda, R) \geq (\frac{3}{R+\lambda+1})$.

(6) When $\lambda = 1$, $\chi_m(P)(Z, 1, R) \geq \frac{1}{\sqrt{Z \times R}}$ and $\chi_m(S)(Z, 1, R) \geq (\frac{3}{R+Z+1})$.

Thus, depending upon the conditions, the above relations can be used to determine the metallic character in a confined or *shell-confined* atom or ion.

-
- [1] M. Somayazulu, M. Ahart, A. K. Mishra, Z. M. Geballe, M. Baldini, Y. Meng, V. V. Struzhkin, and R. J. Hemley, *Phys. Rev. Lett.* **122**, 027001 (2019).
- [2] E. Gregoryanz, C. Ji, P. Dalladay-Simpson, B. Li, R. T. Howie, and H.-K. Mao, *Matter Radiat. Extremes* **5**, 038101 (2020).
- [3] C. Narayana, H. Luo, J. Orioff, and A. L. Ruoff, *Nature (London)* **393**, 46 (1998).
- [4] D. Saumon, G. Chabrier, W. B. Hubbard, and J. I. Lunine, in *Strongly Coupled Plasma Physics*, edited by S. Ichimaru and H. M. Van Horn (University of Rochester Press, Rochester, NY, 1993), pp. 111–120.
- [5] T. Guillot, *Annu. Rev. Earth Planet Sci.* **33**, 493 (2005).
- [6] C.-S. Yoo, *Matter Radiat. Extremes* **5**, 018202 (2020).
- [7] C. Ji, B. Li, W. Liu, J. S. Smith, A. Björling, A. Majumdar, W. Luo, R. Ahuja, J. Shu, J. Wang, S. Sinogeikin, Y. Meng, V. B. Prakapenka, E. Greenberg, R. Xu, X. Huang, Y. Ding, A. Soldatov, W. Yang, G. Shen, W. L. Mao, and H.-K. Mao, *Matter Radiat. Extremes* **5**, 038401 (2020).
- [8] E. Wigner and H. B. Huntington, *J. Chem. Phys.* **3**, 764 (1935).
- [9] K. A. Johnson and N. W. Ashcroft, *Nature (London)* **403**, 632 (2000).
- [10] N. W. Ashcroft, *Phys. Rev. Lett.* **21**, 1748 (1968).
- [11] S. T. Weir, A. C. Mitchell, and W. J. Nellis, *Phys. Rev. Lett.* **76**, 1860 (1996).

- [12] E. Babaev, A. Sudbø, and N. W. Ashcroft, *Nature (London)* **431**, 666 (2004).
- [13] E. Babaev, A. Sudbø, and N. W. Ashcroft, *Phys. Rev. Lett.* **95**, 105301 (2005).
- [14] R. J. Hemley and H.-K. Mao, *Science* **244**, 1462 (1989).
- [15] H. E. Lorenzana, I. F. Silvera, and K. A. Goettel, *Phys. Rev. Lett.* **64**, 1939 (1990).
- [16] M. I. Eremets and I. A. Troyan, *Nat. Mater.* **10**, 927 (2011).
- [17] R. T. Howie, C. L. Guillaume, T. Scheler, A. F. Goncharov, and E. Gregoryanz, *Phys. Rev. Lett.* **108**, 125501 (2012).
- [18] R. T. Howie, T. Scheler, C. L. Guillaume, and E. Gregoryanz, *Phys. Rev. B* **86**, 214104 (2012).
- [19] R. T. Howie, E. Gregoryanz, and A. F. Goncharov, *J. Appl. Phys.* **114**, 073505 (2013).
- [20] P. Dalladay-Simpson, R. Howie, and E. Gregoryanz, *Nature (London)* **529**, 63 (2016).
- [21] M. D. Knudson, M. P. Desjarlais, A. Becker, R. W. Lemke, K. R. Cochrane, M. E. Savage, D. E. Bliss, T. R. Mattsson, and R. Redmer, *Science* **348**, 1455 (2015).
- [22] P. M. Celliers, M. Millot, S. Brygoo, R. S. McWilliams, D. E. Fratanduono, J. R. Rygg, A. F. Goncharov, P. Loubeyre, J. H. Eggert, J. L. Peterson, N. B. Meezan, S. L. Pape, G. W. Collins, R. Jeanloz, and R. J. Hemley, *Science* **361**, 677 (2018).
- [23] K. F. Herzfeld, *Phys. Rev.* **29**, 701 (1927).
- [24] A. Soyulu, *Phys. Plasmas* **19**, 072701 (2012).
- [25] S. Paul and Y. K. Ho, *Phys. Plasmas* **16**, 063302 (2009).
- [26] M. K. Bahar and A. Solyu, *Phys. Plasmas* **21**, 092703 (2014).
- [27] M. K. Bahar, A. Soyulu, and A. Poszwa, *IEEE Trans. Plasma Sci.* **44**, 2297 (2016).
- [28] H. E. Montgomery, Jr., K. D. Sen, and J. Katriel, *Phys. Rev. A* **97**, 022503 (2018).
- [29] S. Paul and Y. K. Ho, *Phys. Plasmas* **15**, 073301 (2008).
- [30] S. Paul and Y. K. Ho, *Phys. Rev. A* **79**, 032714 (2009).
- [31] Y.-D. Jung, *Phys. Plasmas* **2**, 332 (1995).
- [32] Y.-D. Jung and J.-S. Yoon, *J. Phys. B* **29**, 3549 (1996).
- [33] M. Y. Song and Y.-D. Jung, *J. Phys. B* **36**, 2119 (2003).
- [34] F. A. Gutierrez and J. Diaz-Valdés, *J. Phys. B* **27**, 593 (1994).
- [35] J.-S. Yoon and Y.-D. Jung, *Phys. Plasmas* **3**, 3291 (1996).
- [36] L. R. Zan, L. G. Ziao, J. Ma, and Y. K. Ho, *Phys. Plasmas* **24**, 122101 (2017).
- [37] C. Stubbins, *Phys. Rev. A* **48**, 220 (1993).
- [38] N. Mukherjee, C. N. Patra, and A. K. Roy, *Phys. Rev. A* **104**, 012803 (2021).
- [39] B. Saha, P. K. Mukherjee, and G. H. F. Diercksen, *Astron. Astrophys.* **396**, 337 (2002).
- [40] Y. Y. Qi, J. G. Wang, and R. K. Janev, *Phys. Rev. A* **78**, 062511 (2008).
- [41] Y. Y. Qi, Y. Wu, J. G. Wang, and Y. Z. Qu, *Phys. Plasmas* **16**, 023502 (2009).
- [42] Y. Y. Qi, J. G. Wang, and R. K. Janev, *Phys. Rev. A* **80**, 032502 (2009).
- [43] M. Bassi and K. L. Baluja, *Indian J. Phys.* **86**, 961 (2012).
- [44] P. K. Shukla and B. Eliasson, *Phys. Lett. A* **372**, 2897 (2008).
- [45] L. G. Jiao, Y. Y. He, Y. Z. Zhang, and Y. K. Ho, *J. Phys. B* **54**, 065005 (2021).
- [46] C. S. Lam and Y. P. Varshni, *Phys. Rev. A* **6**, 1391 (1972).
- [47] C. S. Lai, *Phys. Rev. A* **26**, 2245 (1982).
- [48] D. Singh and Y. P. Varshni, *Phys. Rev. A* **28**, 2606 (1983).
- [49] R. Dutt, U. Mukherji, and Y. P. Varshni, *J. Phys. B* **19**, 3411 (1986).
- [50] O. Bayrak and I. Boztosun, *Intl. J. Quantum Chem.* **107**, 1040 (2007).
- [51] C. Y. Lin and Y. K. Ho, *Eur. Phys. J. D* **57**, 21 (2010).
- [52] S. Paul and Y. Ho, *Comput. Phys. Commun.* **182**, 130 (2011).
- [53] I. Nasser, M. S. Abdelmonem, and A. Abdel-Hady, *Phys. Scr.* **84**, 045001 (2011).
- [54] A. K. Roy, *Intl. J. Quantum Chem.* **113**, 1503 (2013).
- [55] H. F. Lai, Y. C. Lin, C. Y. Lin, and Y. K. Ho, *Chin. J. Phys.* **51**, 73 (2013).
- [56] Y. Y. Qi, J. G. Wang, and R. K. Janev, *Phys. Plasmas* **23**, 073302 (2016).
- [57] C. Y. Lin and Y. K. Ho, *Comput. Phys. Commun.* **182**, 125 (2011).
- [58] C. G. Diaz, F. M. Fernández, and E. A. Castro, *J. Phys. A* **24**, 2061 (1991).
- [59] S. Lumb, S. Lumb, and V. Prasad, *Phys. Rev. A* **90**, 032505 (2014).
- [60] A. K. Roy, *Intl. J. Quantum Chem.* **116**, 953 (2016).
- [61] Z.-B. Chen, H.-W. Hu, K. Ma, X.-B. Liu, X.-L. Guo, S. Li, B.-H. Zhu, L. Huang, and K. Wang, *Phys. Plasmas* **25**, 032108 (2018).
- [62] M. Belkhir, C. J. Fontes, and M. Poirier, *Phys. Rev. A* **92**, 032501 (2015).
- [63] M. S. Murillo, *Phys. Plasmas* **11**, 2964 (2004).
- [64] Y. Y. Qi, J. G. Wang, and R. K. Janev, *Phys. Plasmas* **24**, 062110 (2017).
- [65] S. Sen, P. Mandal, P. K. Mukherjee, and B. Fricke, *Phys. Plasmas* **20**, 013505 (2013).
- [66] A. L. Efros and D. J. Nesbitt, *Nat. Nanotechnol.* **11**, 661 (2016).
- [67] Z. Fei, Z. Wang, D. Li, F. Xue, C. Cheng, Q. Liu, X. Chen, M. Cui, and X. Qiao, *Nanoscale* **13**, 10765 (2021).
- [68] E. M. Nascimento, F. V. Prudente, M. N. Guimarães, and A. M. Maniero, *J. Phys. B* **44**, 015003 (2011).
- [69] H. Peng, C. Rao, N. Zhang, X. Wang, W. Liu, W. Mao, L. Han, P. Zhang, and S. Dai, *Angew. Chem. Intl. Ed.* **57**, 8953 (2018).
- [70] C. Rao, C. Peng, H. Peng, L. Zhang, W. Liu, X. Wang, N. Zhang, and P. Wu, *ACS Appl. Mater. Interfaces* **10**, 9220 (2018).
- [71] T. Raj kumar, G. Gnana Kumar, and A. Manthiram, *Adv. Energy Mater.* **9**, 1803238 (2019).
- [72] Y. Lai, W. Xia, J. Li, J. Pan, C. Jiang, Z. Cai, C. Wu, X. Huang, T. Wang, and J. He, *Electrochim. Acta* **375**, 137966 (2021).
- [73] M. Fan, D. Liao, M. F. Aly Aboud, I. Shakir, and Y. Xu, *Angew. Chem. Intl. Ed.* **59**, 8247 (2020).
- [74] A.-C. Shi and B. Li, *Soft Matter* **9**, 1398 (2013).
- [75] M. R. Khadilkar and A. Nikoubashman, *Soft Matter* **14**, 6903 (2018).
- [76] G. Gnana kumar, S.-H. Chung, T. Raj kumar, and A. Manthiram, *ACS Appl. Mater. Interfaces* **10**, 20627 (2018).
- [77] W. Shuang, H. Huang, L. Kong, M. Zhong, A. Li, D. Wang, Y. Xu, and X.-H. Bu, *Nano Energy* **62**, 154 (2019).
- [78] J. Wang, L. Zhu, F. Li, T. Yao, T. Liu, Y. Cheng, Z. Yin, and H. Wang, *Small* **16**, 2002487 (2020).
- [79] D. E. Hastings and H. D. H. Stöver, *ACS Appl. Polym. Mater.* **1**, 2055 (2019).
- [80] L. Qin, C. Li, X. Li, X. Zhang, C. Shen, Q. Meng, L. Shen, Y. Lu, and G. Zhang, *J. Mater. Chem. A* **8**, 1929 (2020).

- [81] M. Zhang, C. Xiao, X. Yan, S. Chen, C. Wang, R. Luo, J. Qi, X. Sun, L. Wang, and J. Li, *Environ. Sci. Technol.* **54**, 10289 (2020).
- [82] J. Soullard, R. Santamaria, and J. Jellinek, *J. Chem. Phys.* **128**, 064316 (2008).
- [83] N. Mukherjee and A. K. Roy, *Phys. Rev. A* **104**, 042803 (2021).
- [84] C. Y. Lin and Y. K. Ho, *J. Phys. B* **45**, 145001 (2012).
- [85] M. F. Hasoğlu, H. L. Zhou, and S. T. Manson, *Phys. Rev. A* **93**, 022512 (2016).
- [86] R. D. Woods and D. S. Saxon, *Phys. Rev.* **95**, 577 (1954).
- [87] C. Martínez-Flores and R. Cabrera-Trujillo, *Matter Radiat. Extremes* **3**, 227 (2018).
- [88] Y. B. Xu, M. Q. Tan, and U. Becker, *Phys. Rev. Lett.* **76**, 3538 (1996).
- [89] J. P. Connerade, V. K. Dolmatov, and P. A. Lakshmi, *J. Phys. B* **33**, 251 (2000).
- [90] S. Ichimaru, *Rev. Mod. Phys.* **54**, 1017 (1982).
- [91] A. Ghoshal and Y. K. Ho, *Phys. Rev. E* **81**, 016403 (2010).
- [92] M. Das, *Phys. Plasmas* **19**, 092707 (2012).
- [93] A. K. Roy, *Mod. Phys. Lett. A* **29**, 1450104 (2014).
- [94] A. K. Roy, *J. Math. Chem.* **52**, 1405 (2014).
- [95] A. K. Roy, *Mod. Phys. Lett. A* **29**, 1450042 (2014).
- [96] N. Mukherjee and A. K. Roy, *Intl. J. Quantum Chem.* **118**, e25596 (2018).
- [97] N. Mukherjee and A. K. Roy, *Phys. Rev. A* **99**, 022123 (2019).
- [98] N. Mukherjee and A. K. Roy, *J. Phys. B* **53**, 235002 (2020).
- [99] S. Majumdar and A. K. Roy, *Quantum Rep.* **2**, 189 (2020).
- [100] S. Majumdar and A. K. Roy, *Intl. J. Quantum Chem.* **121**, e26630 (2021).
- [101] M. Das, *Phys. Plasmas* **21**, 012709 (2014).
- [102] A. Dalgarno, *Adv. Phys.* **11**, 281 (1962).
- [103] K. D. Sen, J. Garza, R. Vargas, and N. Aquino, *Phys. Lett. A* **295**, 299 (2002).
- [104] A. Michels, J. deBoer, and A. Bijl, *Physica* **4**, 981 (1937).
- [105] J. Katriel and H. E. Montgomery Jr., *J. Chem. Phys.* **137**, 114109 (2012).
- [106] L. Zhu, Yu. Ying He, L. G. Jiao, Y. C. Wang, and Y. K. Ho, *Phys. Plasmas* **27**, 072101 (2020).
- [107] D. Suryanarayana and J. A. Weil, *J. Chem. Phys.* **64**, 510 (1976).
- [108] E. V. Ludeña, *J. Chem. Phys.* **66**, 468 (1977).
- [109] E. Ley-Koo and S. Rubinstein, *J. Chem. Phys.* **71**, 351 (1979).